# Measuring the Magnetic and Electric Fields of a Microwave Lattice for Atom Chip Development

A thesis submitted in partial fulfillment of the requirement
for the degree of Bachelor of Science in
Physics from the College of William and Mary in Virginia,

by

Sindu E. Shanmugadas

Advisor: Dr. Seth Aubin

Williamsburg, Virginia
January 2022

# Contents

# Acknowledgments

I would like to thank my research advisor Dr. Seth Aubin for suggesting this project to me and for his continous guidance throughout my time at William  Mary. I would also like to thank Dr. Todd Averett and Dr. David Armstrong for their guidance in the senior thesis classes. I would also like to thank the other lab members William Miyahira, Morgan Logsdon, Cate Sturner, and Jordan Shields. Finally I would like to thank my family and friends for all their support. Without all of their support, this thesis would not have been possible.

# List of Figures

**Abstract**

This thesis presents progress on experimental and simulation-based research towards the design, optimization, and characterization of microwave structures for a microwave atom chip to trap ultracold atoms. The purpose of the trap is to create a trapped atom interferometer capable of making precise, localized measurements with long phase integration times. The research consisted of two main thrusts: 1) Measurements of the magnetic and electric components of the near field for a microwave lattice generated by a microstrip transmission line, and 2) microwave simulations of a coaxial cable-to-coplanar waveguide coupler. The measurements on the microwave lattice required the development of several miniature magnetic pickup coils and electric dipole antennas.The magnetic and electric standing wave magnitudes are observed to be roughly 180° out-of-phase, which is consistent with magnetic and electric field components that are 90° out-of-phase. Computer simulations were used to design and optimize a coaxial-to-coplanar waveguide coupler, as well as a tapered coplanar waveguide for focusing microwaves into the 54 $\mu$m wide microstrip traces of the planned atom chip.

# Chapter 1

# Introduction

Optical interferometers, such as the one created by Michelson in the 1880's, can measure small displacements with very high levels of precision. They can be seen in use at LIGO [1], the largest interferometer in the world, which measures gravitational waves. Despite the varying sizes and shapes, they all superimpose beams of light to create interference patterns, which can tell us information about the phenomena acting on the interferometer's light paths, including gravity and inertial forces (i.e rotations and accelerations) [2].

Atom interferometers operate on the same principle as optical interferometers, but replace the optical waves with the matter waves of atoms. Atoms bring two advantages: 1) atomic matter waves can have a much shorter wavelength, thus increasing the interferometer precision, and 2) atoms are directly sensitive to electric, magnetic, and gravitational forces, thus widening the range of phenomena that can be directly measured.

Fermion Interferometery is a form of atomic intereformetry that manipulates the properties of ultra-cold fermions to create a more accurate measuring device. In particular, degenerate Fermi gases (DFG) at ultra-cold temperatures cannot undergo s-wave scattering, due to their anti-symmetric wave functions. As a result, atom-atom collisions are strongly suppressed, thus preventing the interferometer from being sen-

sitive to these detrimental atomic interactions [3]. Scientists in the ultra-cold lab here at William and Mary are interested in building a spin-dependent fermion interferometer for this reason [4]. The challenge lies in splitting atoms into a superposition of spin-up and spin-down states. These atoms are then introduced to a phase (generated by an external force or potential) and then recombined once again. The interference pattern of the interferometer is observed in the change in the ratio of spin-up atoms, which is highly sensitive to the strength of the external force or potential [5]. Scientists in the lab are currently working on building a microstrip-based microwave atom chip to trap the fermion atoms in place in the interferometer. By using trapped atoms, the interferometer benefits by becoming capable of measuring with high spatial resolution and long phase integration time. The mechanism for trapping such atoms is the microwave AC Zeeman effect [4]. A microwave atom chip uses two or three parallel microstrip transmission lines to generate a microwave magnetic near field minimum, which traps the atoms in a tube above the mistrostrips. By using counter-propagating microwaves to create a standing wave along a microstrip (i.e a microwave lattice), the atom can be confined axially as well, while permitting axial positioning over cm-scale distances [4]. The atoms are trapped in a standing wave lattice formation due to the potential created by the interaction with the magnetic field of the microwaves. By changing the phase between the two counter-propagating microwaves, we can control the location of the trap, which occurs at the point of minimum microwave magnetic field.

## 1.1 Objectives and Basic Results

The main objective of the research presented in this thesis is to support the development of a microwave atom chip that can be used to trap atoms for trapped atom interferometry experiments. To this end, the research has focused on two main

objectives: 1) observation and characterization of a microwave lattice in a microstrip transmission line, and 2) the development of a coaxial cable-to-coplanar waveguide (CPW) coupler that can focus microwaves into the atom chip.

These objectives were broadly met during the course of the thesis research, thus providing confidence that once a microwave atom chip is micro-fabricated, then it will work as designed (and simulated). Specifically, this thesis presents the development of miniature magnetic pickup coils and electric dipole antennas for measuring the magnetic and electric fields, respectively, of a microwave lattice. The thesis presents measurements of the lattice's magnetic and electric field components and shows that these are out-of-phase, as expected. Furthermore, the thesis presents the design of a coax cable to CPW connection and simulation-based predictions for the impedance and reflection coefficient for microwaves frequencies of 1-15 GHz. Finally, the thesis presents a design for a tapered CPW for focusing microwaves into the narrow microstrip transmission lines of the atom chip.

## 1.2 Structure of the Thesis

This thesis is structured in the following manner. Chapter 2 presents the basic theory for the physics employed in this thesis. Chapter 3 describes the work and results related to measurements of the microwave lattice's magnetic and electric near fields from various probes. Chapter 4 covers the design and simulations of a coax-to-CPW connection and a tapered CPW. Chapter 5 summarizes the thesis results and provides an outlook for future work.

# Chapter 2

# Theory

This chapter presents the basic physics theory necessary for understanding the experimental results in this thesis, as well as the broader motivation for the work. This chapter is structured in the following manner. We begin by reviewing the theory and operation of a spin-dependent atom interferometer (2.1). Next, we review the theory of spin-dependent AC Zeeman potentials (2.2). The engineering of microwave AC Zeeman potentials is introduced first with a brief description of microstrip transmission lines (2.3) and then the basic design of a microwave atom chip trap (2.4). Finally theory is presented on the basic physics of microwave lattices (2.5), and the magnetic and electric probes for mapping these lattices (2.6).

## 2.1 Spin-Dependent Atomic Interferometry

The proposed spin-dependent interferometer starts out by applying a first "beam-splitter" operation to the atoms that puts each atom into a quantum superposition of spin-up and spin-down states. This operation is accomplished with a "$\pi/2$ pulse" that consists of applying a resonant microwave pulse for a time $\Delta t = \frac{\pi}{2\Omega}$, where $\Omega$ is the Rabi frequency for atomic oscillations between the spin-up and spin-down states. As shown in Fig. 2.1(right), when the microwaves are turned off after a time $\Delta t$, then the probability of an atom to be spin-up is equal to that of being spin-down,i.e. 50-50.

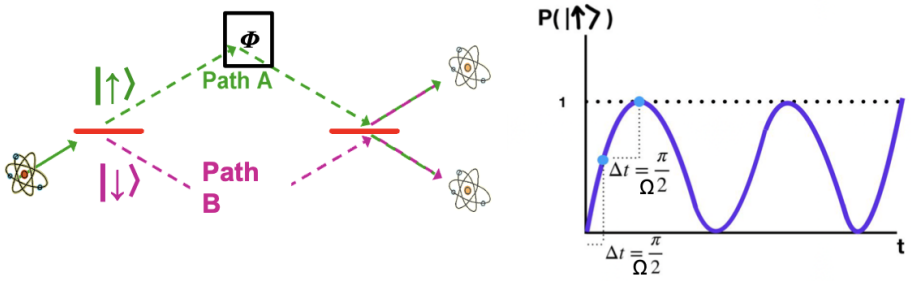


Figure 2.1: Atomic interferometer theory. Left: Diagram of the basic setup for the atom interferometer. One $\Delta t = \frac{\pi}{2\Omega}$ pulse creates an equal superposition of spin-up and spin-down particles, where $\Omega$ is the Rabi frequency of oscillations between the spin-up $|\uparrow\rangle$ and spin-down $|\downarrow\rangle$ states of the atom due to the application of resonant microwaves. Some phase $\phi$ is applied via a gravitational field, object, magnetic field, gradient etc, and then the atoms are recombined. Finally, another $\frac{\pi}{2\Omega}$ pulse is applied. The ratio of spin up atoms to total atoms is then measured versus the changes in $\phi$, e.g. by varying varying the height $h$ between the two spin paths (and thus varying the potential energy difference $mgh$) Right: This plot sketch outlines the sinusoidal Rabi oscillation for the probability for an atom to be in the spin-up $|\uparrow\rangle$ state (at $t = 0$ the atom is in a pure spin-down $|\downarrow\rangle$ state). The $\Delta t$ labeled represents one $\frac{\pi}{2\Omega}$ pulse. When we turn off the microwave current at this time $\Delta t$, each atom is in an equal superposition of spin-up and spin-down states (50-50 superposition).

Therefore, each atom is put into a 50-50 superposition of spin-up and spin-down by the first beamsplitter operation. Next, the spin-up and spin-down components of each atom are directed along two spatially distinct paths (as shown in Fig. 2.1(left)), where they acquire a relative phase $\phi$ between them due to a spatial difference in potential energy (due to a gravitational, electric, or magnetic field, or an inertial force). After a phase integration time $t$, the two paths (and spin states) are recombined on a second "beamsplitter", and the phase is read-out from the final ratio of spin up atoms to the total atom number. It should be noted that the spin-up and spin-down components of each atom are directed along different paths (path A and path B, respectively, in Fig. 2.1(left)) by two spin-specific microwave traps that follow these paths. After the first pulse, the traps for the spin-up atomic component and the spin-down atomic

component travel along different paths that are then exposed to a spatially dependent external potential energy field (i.e an external force) that induces a phase difference $\phi$ (and ultimately modifies the spin-up population ratio at the read out). The atoms are then recombined and another $\pi/2$ pulse is applied which should produce atoms fully in spin-up in an undisturbed (no $\phi$) system. The wavefunction then looks like:

$$|\Psi(t)\rangle = e^{\frac{-iE_{\uparrow A}t}{\hbar}}|\uparrow\rangle|A\rangle + e^{\frac{-iE_{\downarrow B}t}{\hbar}}|\downarrow\rangle|B\rangle \tag{2.1}$$

where $|A\rangle$ and $|B\rangle$ refer to the spatial states for paths A and B, respectively. Factoring out the time evolution exponential on the $|\uparrow\rangle|A\rangle$ term in eq. 2.1, then the phase $\phi = \frac{DeltaEt}{\hbar}$ appears:

$$|\Psi(t)\rangle = e^{\frac{-iE_{\uparrow}At}{\hbar}}[|\uparrow> |A\rangle + e^{\frac{-i\Delta Et}{\hbar}}|\downarrow\rangle|B\rangle] \tag{2.2}$$

In the case of an interferometer configured for measuring the local strength of gravity, we have $\Delta E = E_{\uparrow A} - E_{\downarrow B} = E_{hfs} + mgh$. Here, $E_{hfs}$ is the hyperfine splitting energy between the spin up and spin down states (e.g. 6.8 GHz in $^{87}$Rb), and $mgh$ represents the difference in gravitational potential energy between paths A and B. The interferometer signal $S$ is given as:

$$S = \frac{N_{\uparrow}}{N_{\uparrow} + N_{\downarrow}} \tag{2.3}$$

Where $N_{\uparrow}$ represents number of spin-up atoms after the two pulses, and $N_{\downarrow}$ represents the number of atoms spin-down atoms after recombining the paths and application of the second beamsplitter $\pi/2$ pulse.

This spin-dependent interferometer requires a mechanism for directing and trapping spin-up and spin-down atoms along two different paths (A and B). An AC Zeeman potential can provide such a spin-dependent mechanism.

## 2.2 Spin-Dependent AC Zeeman Potentials

The AC Zeeman potential energy for an atom in a microwave magnetic field $\vec{B}_{ac}$ is given:

$$E_{\pm} = \pm\frac{\hbar}{2}(-|\delta| + \sqrt{\delta^2 + |\Omega|^2}) \tag{2.4}$$

Here $\Omega(\vec{r}) = \langle g|-\vec{\mu}\cdot\vec{B}_{ac}(\vec{r})|e\rangle/\hbar$ is the Rabi frequency and $\vec{\mu}$ is the magnetic moment of the atom. Additionally, the detuning $\delta = \omega - \omega_{\downarrow\uparrow}$ is the frequency difference between the microwave field frequency $\omega$ and the atomic transition frequency $\omega_{\downarrow\uparrow} = E_{hfs}/\hbar$ [4] [6]. As shown in Fig. 2.2, when the microwave frequency is less than $E_{hfs}$, $\delta < 0$ and the atom's energy gap widens, while in the other case, $\delta > 0$ and the energy gap decreases. If an atom's spin energy level is higher in the presence of a microwave field, then the associated atomic spin state becomes a low-field seeker, since it can minimize its energy by travelling to where the microwave field is lowest (see Fig. 2.2). Similarly, if an atom's spin energy level is lower in the presence of a microwave field, then this atomic spin state becomes a high-field seeker. Therefore, a local minimum in the microwave magnetic field can be used to trap low-field seeking spin states, while a local maximum in the field can be used to trap high-field seeking spin states. An AC Zeeman trap is spin-specific (i.e. traps only a given spin state), and the strength of the trapping potential is determined by the power and frequency (i.e. detuning $\delta$) of the microwave source [7].

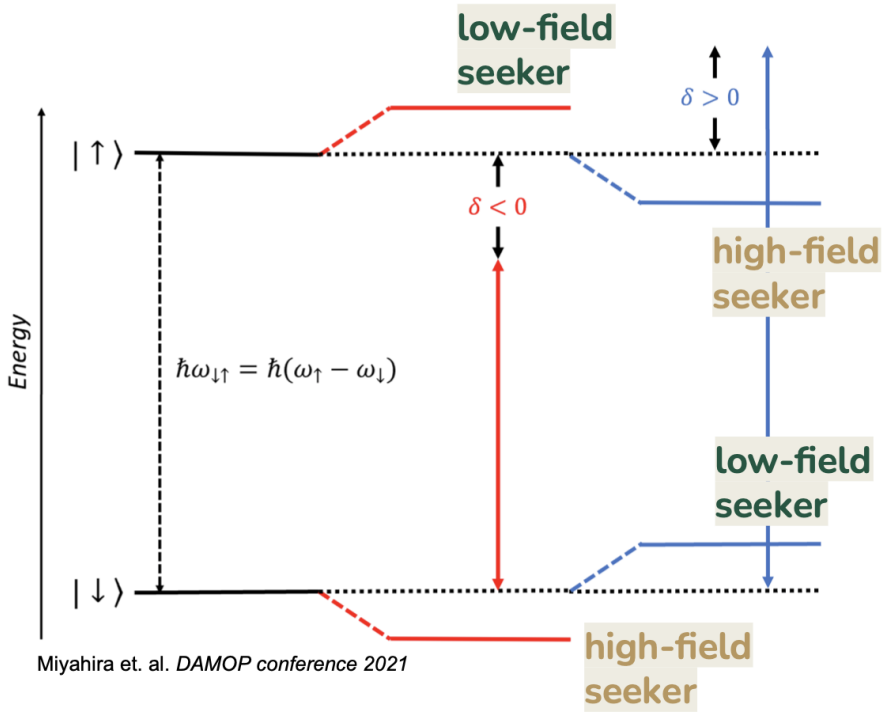


Figure 2.2: AC Zeeman energy level shifts for a two-level atom. The energy levels for the $|\uparrow\rangle$ and $|\downarrow\rangle$ states are pushed apart when the microwave field is red-detuned ($\delta < 0$) and pulled together for blue-detuning ($\delta > 0$). Figure adapted from ref. [3]

## 2.3 Microstrip Transmission Line

A microstrip transmission line can be used to generate a microwave magnetic ear field (quasi-TEM mode). A microstrip has a fixed broadband impedance (often 50 Ω) and consists of a ribbon trace conductor on a dielectric substrate with a conducting ground plane. The microstrip transmission line in Fig. 2.3 has a 50 Ω impedance and consists of a 50 $\mu$m thick aluminum nitride substrate ($\epsilon_r = 8.9$) (blue) with a copper groundplane (bottom face) and a 54 $\mu$m wide copper trace (red). At one end of the trace, a 50 Ω voltage source is inserted, and on the other end there is a 50 Ω load. The microwaves can be applied in the range 1-15 GHz, though we typically target

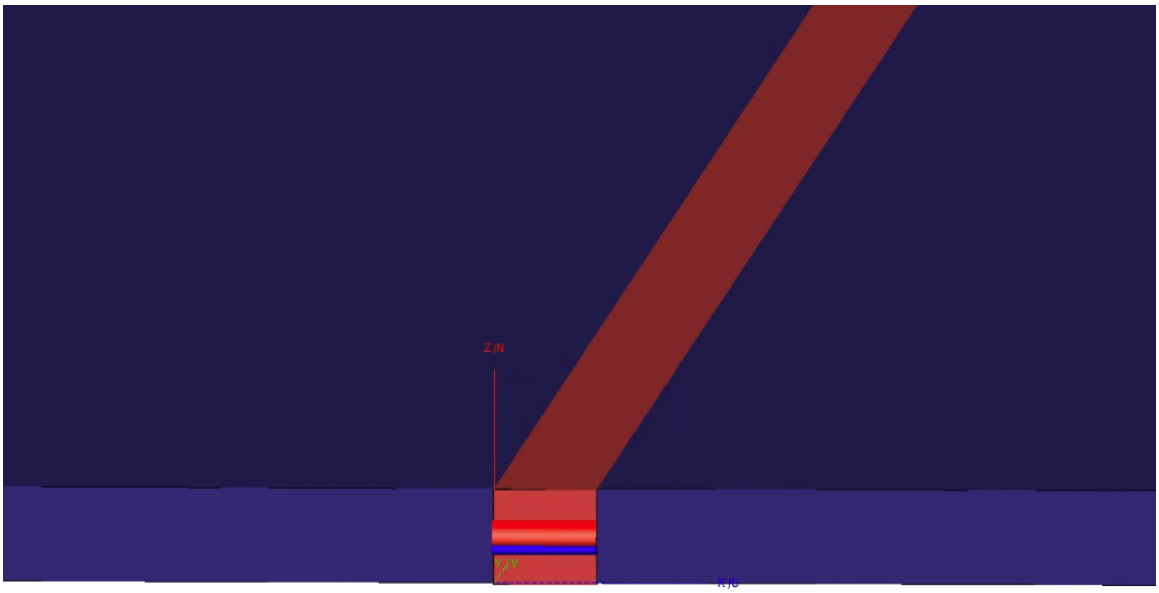

Figure 2.3: Basic setup for a microstrip transmission line. The red rectangle is the copper trace, and the blue rectangular region is the aluminum nitride (AlN) dielectric substrate. A copper ground plane on the bottom of the substrate is not visible.

$E_{hfs,Rb87}/h = 6.8$ GHz. The setup shown in Fig.2.3 is used to create an atom-trapping microwave chip. In the experimental setup used for the work in this thesis, we used a used a $\frac{1}{16}$" FR4 substrate ($\epsilon_r = 4.4$).

## 2.4 Microwave Atom Chip Trap Design

Once fabricated, the microwave atom chip will consist of a thin dielectric substrate (aluminum nitride, i.e. AlN) with a copper groundplane on one side. On the other side of the substrate, two or three parallel copper traces (54 $\mu$m wide) will be deposited by a photolithographic process [8]. The microwave field traps atoms via the AC Zeeman effect, which can draw atoms towards either a local microwave field maximum or a minimum. In the case of the chip-based trap, the atoms are trapped by a minimum in the microwave magnetic near field (Earnshaw's theorem ensures that only a field

minimum can be generated in the near field).

The AC Zeeman effect will trap the atoms in the magnetic minima as shown in Fig.2.4. The total microwave magnetic field is the sum of the near fields from the currents in the left and right traces and the center trace, which is 180° out-of-phase. Additionally, the atoms are axially confined with a standing wave produced by microwave sources of equal power at opposite ends of the center trace. My research focuses on making sensors to measure the electric and magnetic fields of the microwave standing wave, in order to characterize and adjust the axial atom trap.

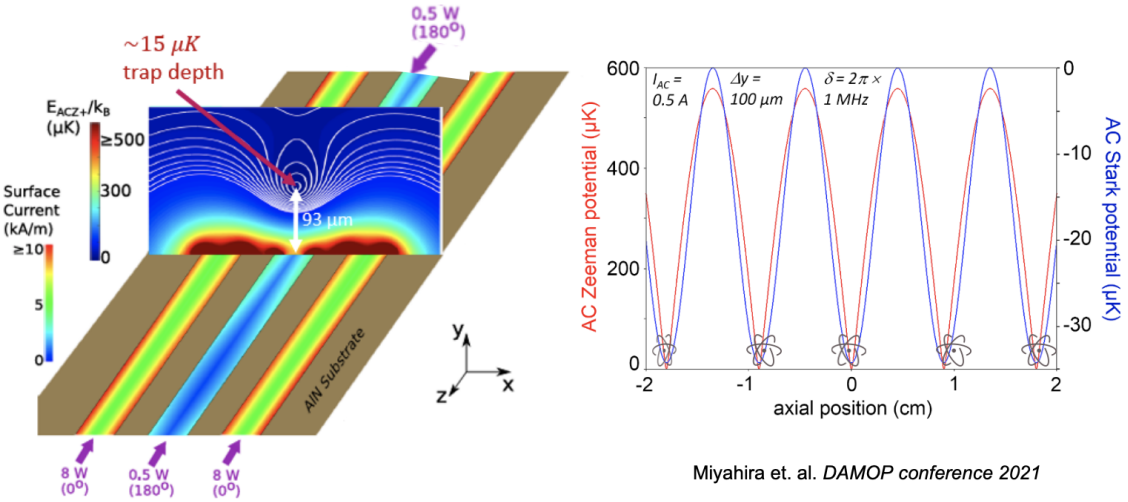


Figure 2.4: Simulation of the microwave trap where the atoms are low-field seekers and are trapped in the microwave minima. Left: Transverse confining potential. Right: Axial confining potential due to a microwave lattice. Figure from ref [4].

## 2.5 Standing Wave Theory

The microwave lattice trap relies on a microwave standing wave generated by two counter-propagating microwaves. A standing wave is one that does not translate with change in time, but remains stationary in space with only changes in the amplitude. Let us consider a standing wave generated by a travelling wave incident on a perfect

conducting mirror. We define the electric and magnetic components of the incident plane wave as:

$$\vec{E}_I = E_0 e^{i(kz-\omega t)}\hat{x} \tag{2.5}$$

$$\vec{B}_I = B_0 e^{i(kz-\omega t)}\hat{y} \tag{2.6}$$

where $k = 2\pi/\lambda$ is the wavevector number for a wave of wavelength $\lambda$ propagating along the $+\hat{z}$ direction, and $\omega$ is the frequency of the wave (in rads/s). The electric and magnetic field amplitudes for the wave are given by $E_0$ and $B_0$, respectively, and are related by $B_0 = E_0/c$, where $c$ is the speed of light in the medium. Upon reflection from the mirror (located at z=0 in the $xy-$plane), the electric and magnetic components of the reflected wave are given by

$$\vec{E}_R = -E_0 e^{i(-kz-\omega t)}\hat{x} \tag{2.7}$$

$$\vec{B}_R = B_0 e^{i(-kz-\omega t)}\hat{y} \tag{2.8}$$

Then, the total real part of the electric field is given by $\vec{E}_{total} = 2E_0 sin(kz)sin(\omega t)\hat{x}$. The total electric field has the time-dependent sine term separate from the spatial $z$ dependent sine term. Therefore, for a given frequency $\omega$, the amplitude of the wave varies sinusoidally in time, but the wave does not travel (i.e. shift) along the $z-$axis and instead remains stationary. Therefore, we have a standing wave (it does not travel). Repeating this for the real part of the magnetic field we have: $\vec{B}_{total} = 2B_0 cos(kz)cos(\omega t)\hat{y}$ . Thus, the total magnetic field is also a standing wave. If we compare the total electric and magnetic field equations, we see that they are exactly $\pi/2$ out of phase in space and time, as shown in 2.5. In the microwave trace setup described in the next chapter, instead of having a mirror create a reflected-incident wave interaction, we have two identical, but counter-propagating waves coming from either end of the trace. This arrangement creates the same scenario, and therefore we

should have standing waves for both the magnetic and electric fields of the microwave lattice.

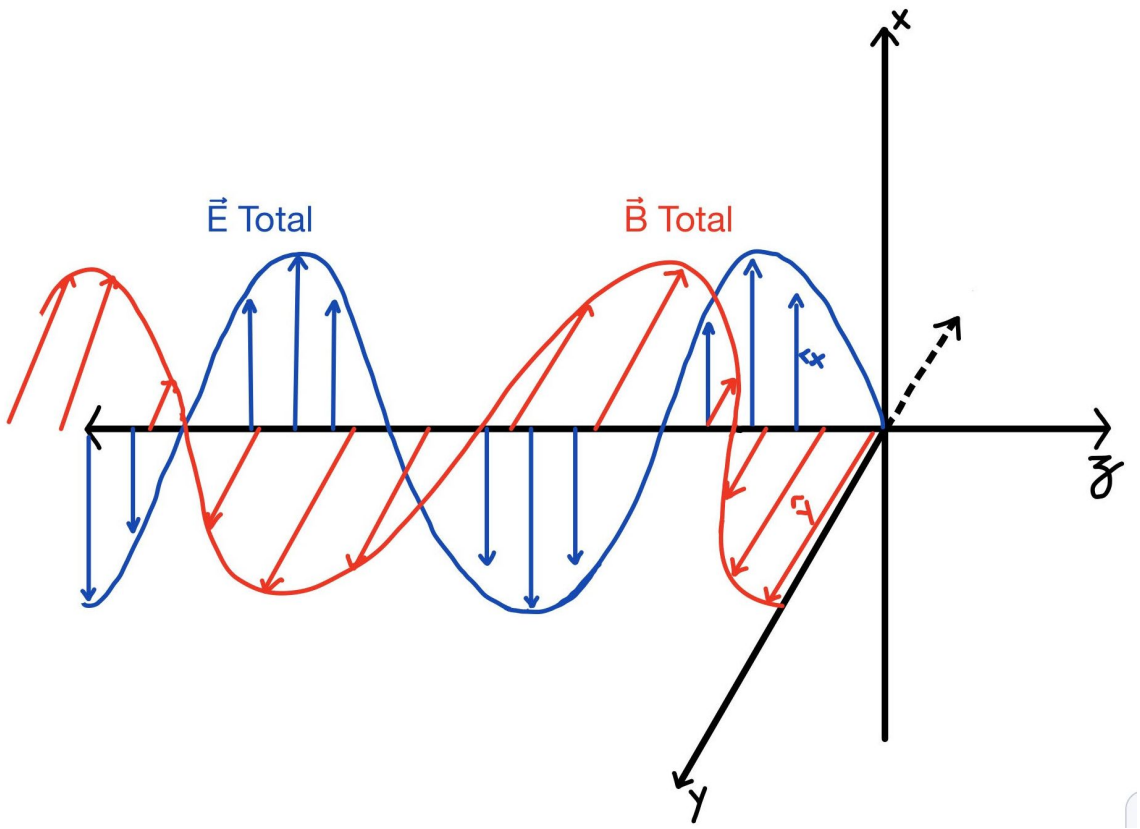


Figure 2.5: Plot sketch of the total magnetic and electric fields of a standing wave. The magnetic field total ($\vec{B}_{total}$) is a cosine-wave in the y-z plane and the electric field total ($\vec{E}_{total}$) is a sine-wave in the x-z plane. The waves are $\frac{\pi}{2}$ out of phase in both space and time.

### Magnetic and Electric Field Measurements using Spectrum Analyzer

While the electric and magnetic fields of a standing wave are 90° out-of-phase in space and time, when we make measurements of the electric and magnetic field strengths we see a spatial phase shift consistent with 180°. We probe the field strength with a spectrum analyzer. The spectrum analyzer measures the power spectral density, i.e. electromagnetic power in a given frequency bin. The power P at a given frequency is measured in dBm typically and contains no temporal phase information. The power is given by $P^2 = \frac{V^2}{R}$, where V is the voltage of the probe signal and R is the impedance

of the transmission line (i.e. 50 Ω). Depending on the type of probe used, $V^2$ is proportional to either $E^2$ or $B^2$ (or some combination of these, depending on the fidelity of the probe).

If we square the $E$ and $B$ equations for the standing wave in the previous section, then we get:

$$E^2 = cst1 * sin(kz)^2 = cst1 * 0.5[1 - cos(2kz)] \tag{2.9}$$

where $cst1$ represents the time dependent term squared, which when time averaged becomes the amplitude for measured spectrum analyzer signal. Similarly, the equation for the magnetic component $B$ of the standing wave becomes:

$$B^2 = cst2 * cos(kz)^2 = cst2 * 0.5 * [1 + cos(2kz)] \tag{2.10}$$

Therefore, $E^2$ and $B^2$ have spatially oscillating parts which correspond to a 180 degree phase shift as measured by the spectrum analyzer. The "2kz" term in the cosine means that the wavelength measured by the spectrum analyzer is actually half the wavelength of the actual $\vec{E}$ or $\vec{B}$ fields. When the spectrum analyzer measures a signal in $mV$ it is essentially taking the square root of the power which is proportional to $|E|$ or $|B|$ and this still would shows a phase shift of 180 degrees.

## 2.6 Magnetic and Electric Field Probes for the Microwave Lattice

The magnetic and electric components of a microwave field can be detected using a pickup coil and a small dipole antenna, respectively.

### Pickup Coil

The theory presented for the pickup coil is accurate at low frequencies, i.e. Hz - MHz, but it can but can still be applied to a pickup-coil for microwaves, despite

neglecting effects from impedance matching. The basic setup is a conductive wire such as copper bent into a singular loop. For microwaves frequencies, some degree of impedance matching can be obtained by stripping a coaxial cable down to its center conductor, which is then looped back to the outer ground sheath. The loop is placed axially perpendicular to the length of the trace, as by the right hand rule, we see that the magnetic field created from the interaction of the microwaves will primarily circulate around the trace (in a plane perpendicular to the trace). By Faraday's law we get,

$$V_{coil} = -\frac{d}{dt}(\vec{A} \cdot \vec{B}) = iAB\omega \tag{2.11}$$

Where $\vec{B} = \vec{B}(x, y)e^{-iwt}$ represents the magnetic field in the microwave lattice, $\vec{A}$ is the area of the pickup coil, and $\omega$ is the frequency of the source [9]. If the pickup coil is very close to the trace, then equation 9 becomes:

$$V_{coil}(x) \approx i\omega A\frac{\mu_0}{2}J(x) \tag{2.12}$$

using Ampere's law in the quasi-static limit and taking the pickup coil to be approximately along the surface of the trace [9]. Therefore, there is a direct relation between the voltage induced on the coil, which is then picked up by the spectrum analyzer, and the magnetic field produced by the microwave lattice system.

**Dipole Antenna**

A dipole antenna consist of two short colinear wire stubs that are in-line with each other but are opposite to one another. We denote $d$ the separation between the wire stubs (or the center-to-center separation between the stubs). In the low frequency limit, the electric field component $E$ along the axis of the antenna (i.e. of the wires) is related to the voltage difference$V_{dipole}$ between the wires by $V_{dipole} = dE$. In the microwave case, it is convenient to construct the dipole antenna from a coaxial cable

by stripping the center conductor to form a short wire stub and bending it perpendicular to the cable. The second wire stub can be formed from the ground sheath (and bending it perpendicular to the cable also, but in the opposite direction from the center conductor stub) [10]. In a microstrip, the electric field lines emanate perpendicular from the trace, so the wire stubs of the dipole antenna should also be oriented perpendicular to the trace to measure the microwave electric field.

# Chapter 3

# Microwave Lattice Measurements

This chapter presents the measurements on the microwave lattice. More specifically, section 3.1 describes the basic apparatus for the measurements, while section 3.2 details the measurements as well as methods for minimizing performance difficulties. Section 3.3 presents observations regarding the impact of placing various materials in the vicinity of the microwave lattice. Sections 3.4-3.5 present results from the fabrication of magnetic and electric field sensors from from the thin "Mouser" coaxial cable. Finally, sections 3.6-3.7 cover results from sensors fabricated from the smaller copper coaxial cable.

## 3.1 Measuring the Magnetic Fields of Microwave Lattice with First Pickup Coil

The first step of my project was to measure the magnetic fields using the pickup coil already available in the lab. The coil used (referred to as blue sensor/probe) is a microwave coaxial cable with a center copper conductor covered with a dielectric material plastic (polyethylene) and then a conducting sheath on top (braided wires) with a blue cladding material (Mini circuits cable, part 141-12SM+). The part of the sensor near the trace has no cladding, and so a circular loop of wire is exposed.

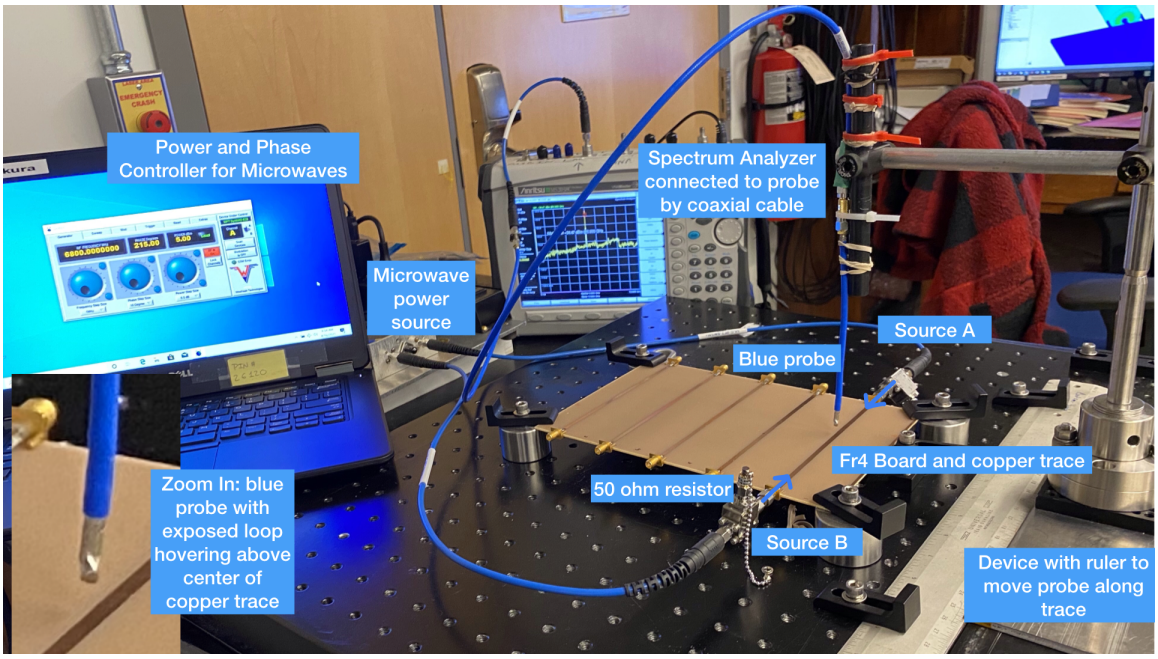


Figure 3.1: Setup for measuring the magnetic field of the microwave lattice. This is the basic setup where the sensor (i.e. the blue pickup coil) is attached to a metal rod which can move along a ruler, which is screwed in place, to properly record position. We used a $\frac{1}{16}$" thick FR4 board with a 14 cm long and 3 mm wide copper trace. Microwaves are fed into both sides through coaxial cables connected to a dual-output source controlled by software. Both outputs' frequencies were kept at 6.8 GHz but phase and power were varied in different trials. Each of the microwave sources has a 50 Ω output impedance. The input to each side of the microstrip has a circulator to avoid reflections and suppress signals going from one source into the other (one of the three circulator ports is terminated with a 50 Ω resistor).

The setup for measuring the microwave lattice is shown in Fig.3.1 We proceeded to take several data collections aiming to measure the magnetic field of the microwave lattice at various phase differences and compare the results to previous ones done in the lab. We first adjusted the device to place the pickup coil at the center of the trace. We then translated it along the trace, checking to make sure it travels in a straight line.

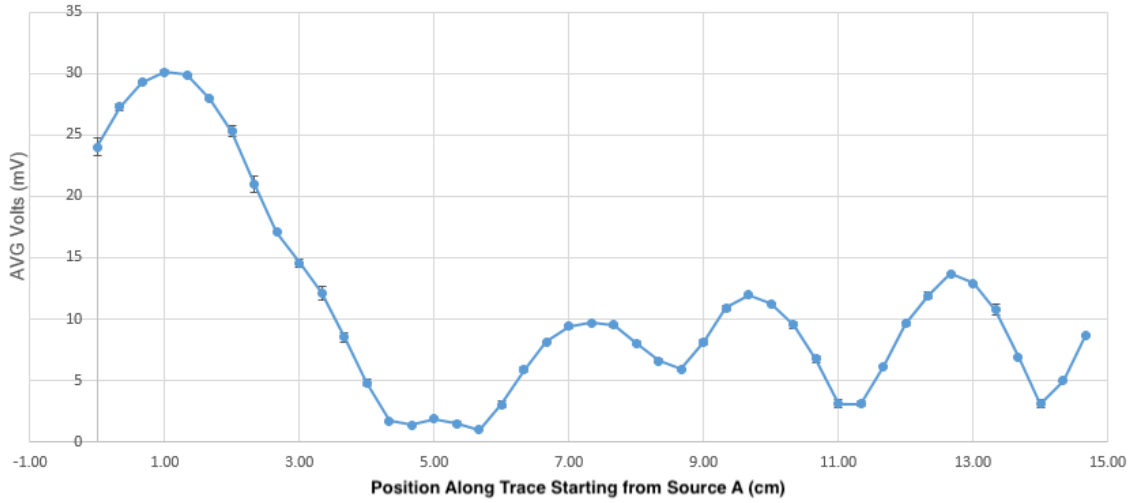


Figure 3.2: Probe signal versus position for initial microwave lattice measurement. We took two trials for the traces here with a 0 degree phase difference. The vertical error bars represent the standard deviation between the results which was very small, indicating that the lack of a standing wave was due to improper setup of the device or inaccuracy in the sensor capabilities for the blue pickup coil. The plot shows the data points taken as well as a guide line to the eye (not a fitted curve).

## 3.2 Results for the Blue Pickup Coil Sensor

The data taken should show a standing wave for the magnetic field if the two counter-propagating microwave signals have the same power. However, through multiple trials, we found that the data was not reproducible nor was it producing a standing wave with a similar wavelength compared to older results taken by the lab. The preliminary results for the "blue" pickup coil are shown in Fig.3.2:

It is important to define orientation of the pick up coil and dipole antenna shown later in the thesis. The direction of the coil with respect to the trace is defined as the normal vector to the loop's area. The orientation is "parallel" when the normal vector is in the same direction as microwave current and "perpendicular" when the normal vector is perpendicular to the microwave current. These definitions are depicted in Fig.3.3

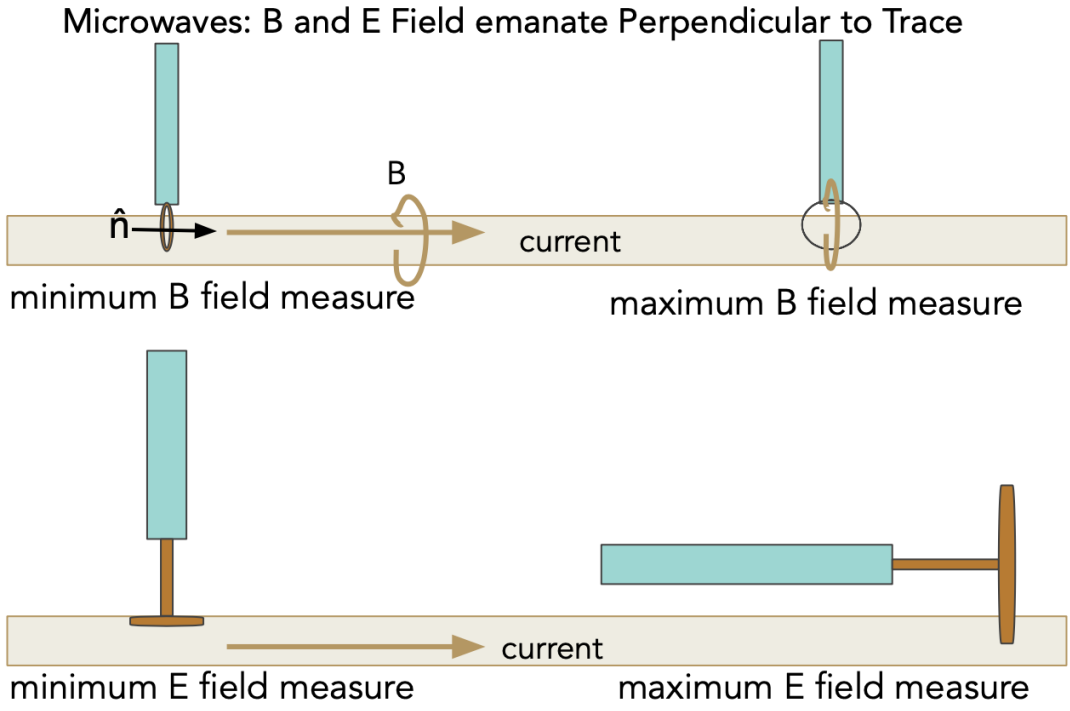


Figure 3.3: Pickup coil and dipole antenna orientations. From the right hand rule, it is inferred that when a loop's area vector ($\hat{n}$) is perpendicular to the direction of current, maximum magnetic field ($\vec{B}$) is measured, and when $\hat{n}$ is parallel to current direction, minimum $\vec{B}$ is obtained. For a microwave system, the maximum electric field is also perpendicular to the trace, and so it is oriented vertically above the trace. Therefore, a maximum $\vec{E}$ is measured when the poles are oriented perpendicular to the current direction (trace) and a minimum when pole orientation is along the current direction.

The first issue that we noticed with the pickup coil sensor was that turning the loop from its perpendicular orientation to a parallel one along the length of the trace had no effect on its reading, suggesting that what it measures is not necessarily the magnetic field of the microwave lattice. The data also had very few humps indicating a longer wavelength for the standing wave than it should be according to simulation. To trouble shoot, we took trials of one source either connected to nothing or to a 50 Ω resistor.

Theoretically, a 50 Ω microstrip trace connected a 50 Ω source on one end and

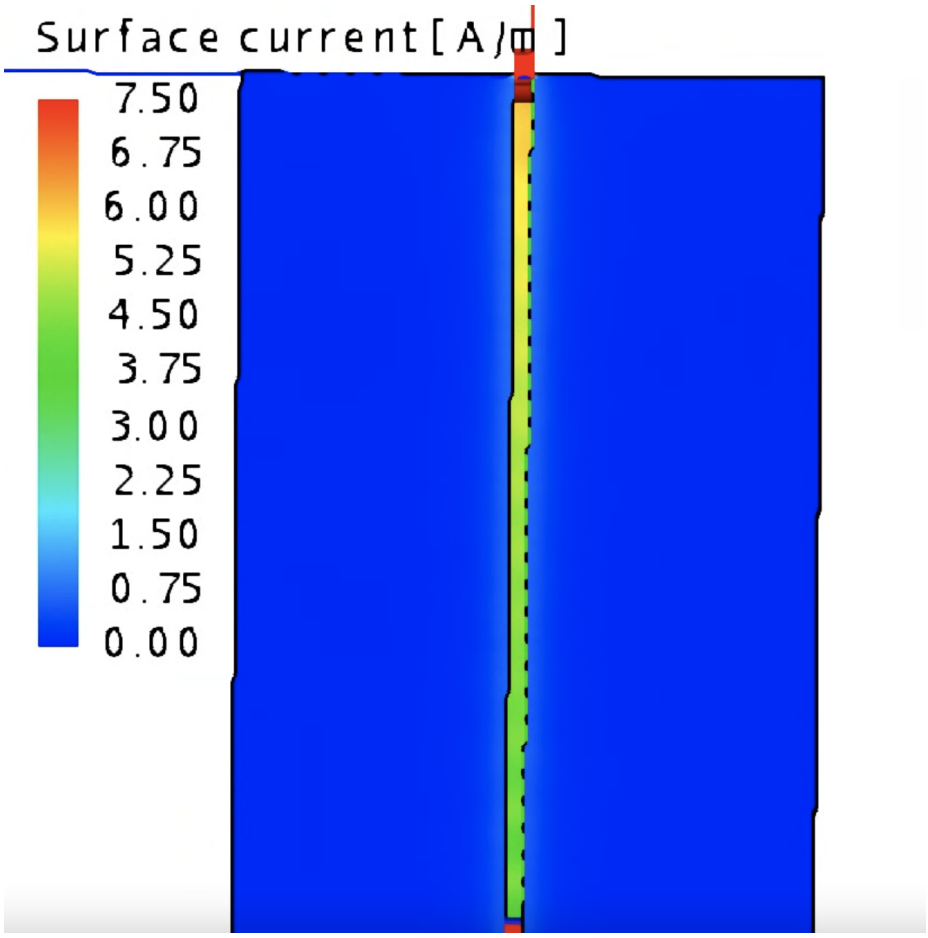


Figure 3.4: Current density in a microstrip trace with a single travelling wave entering at the top (50 Ω source port with 1 V amplitude) and absorbed at the bottom in 50 Ω load. Here the trace is 15.2 cm long with a 3 cm copper trace width on a FR4 substrate.

50 Ω load on the other end would just have a single travelling wave, and so it should have the same current amplitude and magnetic field amplitude all along the trace. Using microwave simulations (FEKO by Altair Inc.), we see that there will some loss, but the current does follow this pattern as shown in Figure 3.4.

However, as shown in Fig.3.5 below, measurement trials with both sources separately connected to 50 Ω loads did not produce the uniform results of Fig.3.4. These

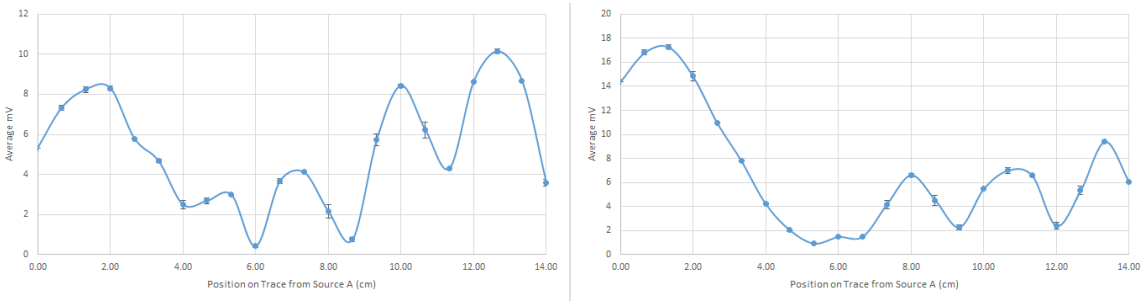


Figure 3.5: Single microwave source connected to trace with a 50 Ω load. Left: Source connected to the B side of the trace with a 50 Ω load on the A side. Right: Source connected to the A side of the trace with a 50 Ω load on the B side. In both cases, we do not have a uniform constant reading (with minimal loss). In the right plot, there is a general loss which is a bit more promising, however in both trials there is some sort of interaction with the pickup coil that is creating a semi-sinusodial like wave. The data was also done twice in both cases with the standard deviation as the vertical error bars being quite low, again suggesting a problem with the fidelity and accuracy of the blue pickup coil probe. The plots show data point taken as well as a guide line to the eye (not a fitted curve).

results suggest a measurement method issue, including the possibility of some interaction between the trace and the pickup coil that is warping results.

In the case of a single source connected to nothing on the far end, the microwave should be fully reflected back (with some loss) and interact with the source wave causing a standing wave formation. This behavior was shown in the simulation data as well (see Fig.3.6), producing a standing wave when we shifted through the phases for the instantaneous magnitude, despite a slight translation of the wave down the trace. However, as shown in the measurement trials of Fig.3.7, both sources separately connected to nothing on the other end did not produce this result, suggesting some interaction between the trace and the pickup coil warping results or some other issue.

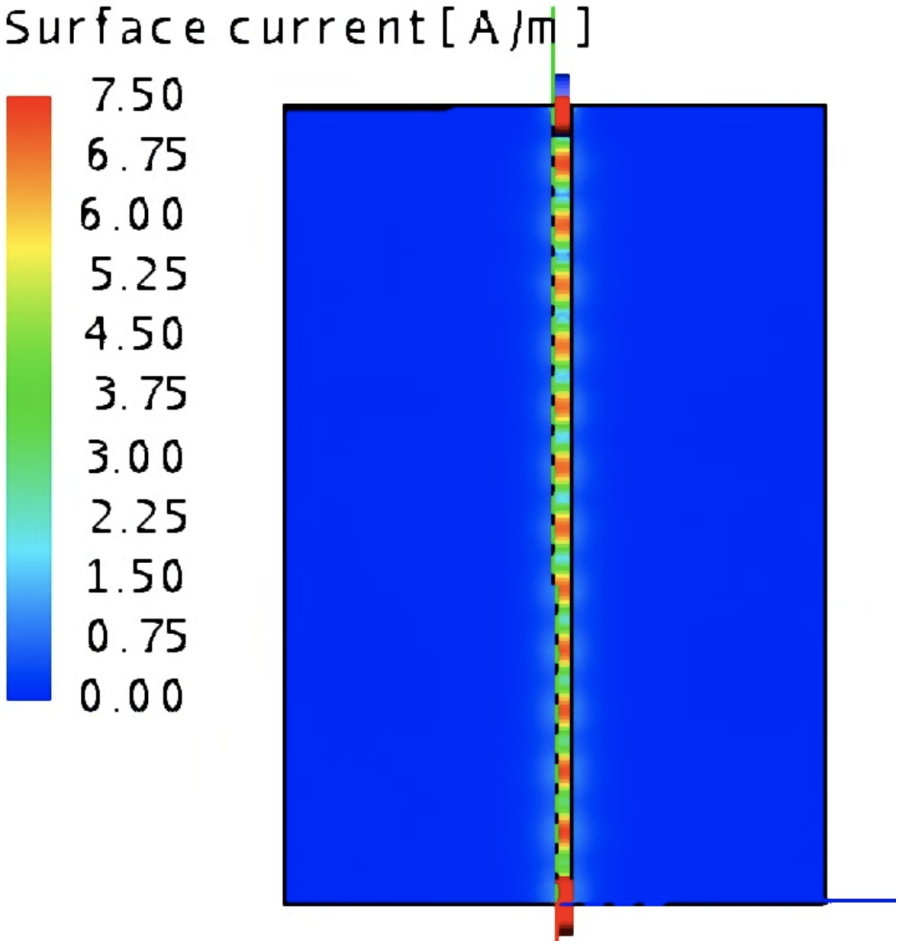


Figure 3.6: Simulation of the current density for the measurements in Fig.3.7. As expected, the setup produced a standing wave in simulation. The wavelength is approximately 2.18 cm. Here the trace is 15.2 cm long with a 3 cm copper trace width on a FR4 substrate.

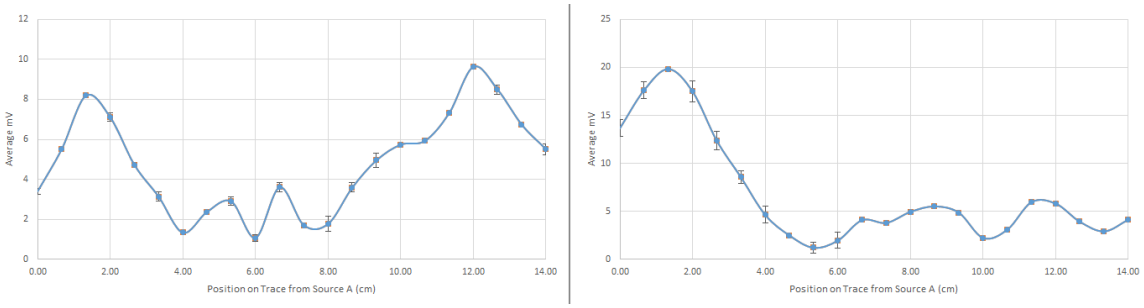


Figure 3.7: Single microwave source connected to nothing on other side of trace. Left: Source connected to the A side of the trace with no load on the B side. Right: Source connected to the B side of the trace with no load on the A side. Magnetic field pickup coil (blue coil) data for a single source with no load (nothing) connected to the output of the microstrip trace. There is no obvious sinusodial wave relation, as it does not follow a clean repeating standing wave. Both plots show the data points taken as well as a guide line to the eye (not a fitted curve).

The inconsistencies between theory and simulation with the experimental results indicates an issue with the blue coil's ability to take accurate data, or perhaps indicates a larger problem. Nevertheless, we wanted to try and optimize this system the way it is.

### 3.2.1 Power-balancing and Phase Trials

The difficulties with the data indicated that perhaps the two microwave sources were not balanced in power. The next section covers the method and results for attempting to power balance the sources to produce a more accurate result.

We first directly connected each microwave source (A and B) into the spectrum analyzer, and found that they were working properly and are controllable with the software in terms of their phase, power, and frequency respectively.

Though both sources were set to an output power of 10 dBm, the previous trials indicated that the sources may not be power balanced. We first tried solely power

balancing the sources by parking the pickup coil sensor at the axial center of the trace, and adjusting each source's power so that they read the same amplitude (mV) on the spectrum analyzer. This however, produced varying power balancing, as at different points along the trace, there was high variation in the power needed in each source to balance their outputs. This again indicated the difficulty in developing accurate and reproducible results using the blue pickup coil.

The other indication of proper power balancing was to direct both sources into the trace (via the two end ports) and to park the sensor along various points along the trace and shift through the phase. If the sensor picks up a sinusodial wave that goes down to nearly 0 mV and back up again, then it is a good indicator for proper power balancing. Through several tests at various points along the phase, we found that the variability in the output of the analyzer changed. Meaning, some areas produced a good sine wave that went to nearly 0 mV while other areas varied in a form somewhat of a sine wave, however, never fully reaching near 0 mV. This again, indicated some loss in our system, as well as inaccuracies in the use of the blue pickup coil.

Since, both methods still had some error in showing a proper power balancing, we ended up using both: First, we parked the probe in the center of the microstrip trace and power balanced the sources to produce equal amplitude signals at the probe; second, we ran through the phase at different points along the trace to verify that we obtained a sine wave that goes to 0 mV and then back up again within 0-360 degrees.

Using this method, we found the power balancing to be best for 5 dBm on source A and 10 dBm on source B. We then ran the phase trial at 7.5 cm from the source A SMA port, which in phase trials was shown to be a spot along the trace with proper phase results going to 0 mV and back up again when shifting through the phases. We additionally ran the phase trial at 2.7 cm from the SMA port for source A, which we found in the previous phase trial to produce the least variability in the output when

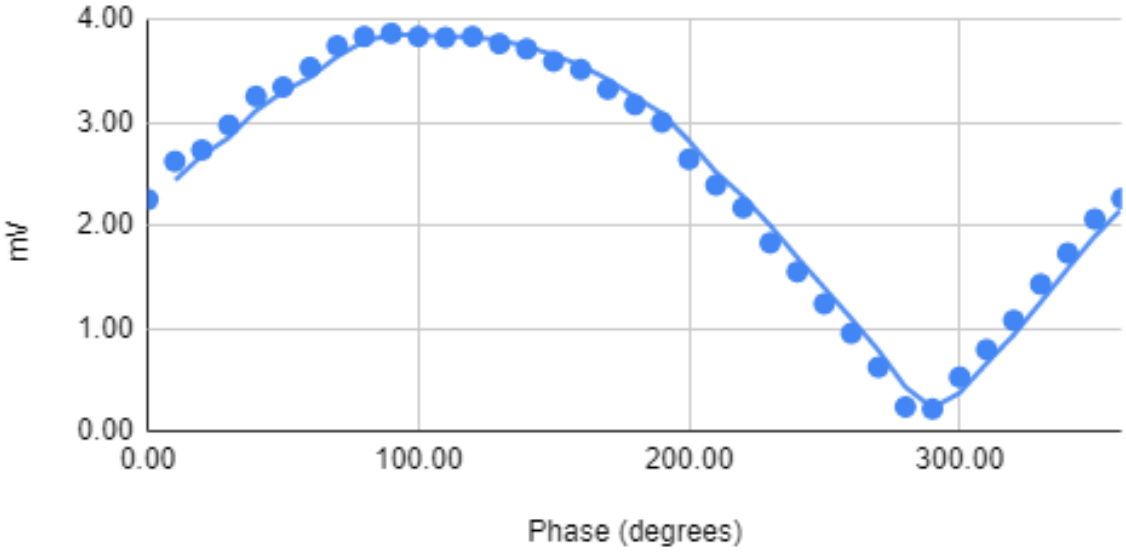


Figure 3.8: Microwave lattice strength versus phase with probe 7.5 cm from source A. The phase data indicates a good power balancing between the traces, as it follows a sinusodial pattern that heads towards nearly 0 mV and back up again in 360°. Figure shows the data points taken as well as a guide line to the eye (not a fitted curve).

shifting phase. The results are shown below in Fig.3.8:

Having completed the power balancing procedure, the microwave lattice measurement trial of the pickup coil signal versus position is repeated, i.e. same measurement as Fig.3.2 but with power balancing. The results of these measurements are shown in Fig.3.9 below, along with previous lab measurements by A. Rotunno and D. Beringer:

Next, we took the data with this power balancing for different for different relative phases between sources A and B to see if the standing wave data translates in space as the phase is varied (see Fig.3.10).

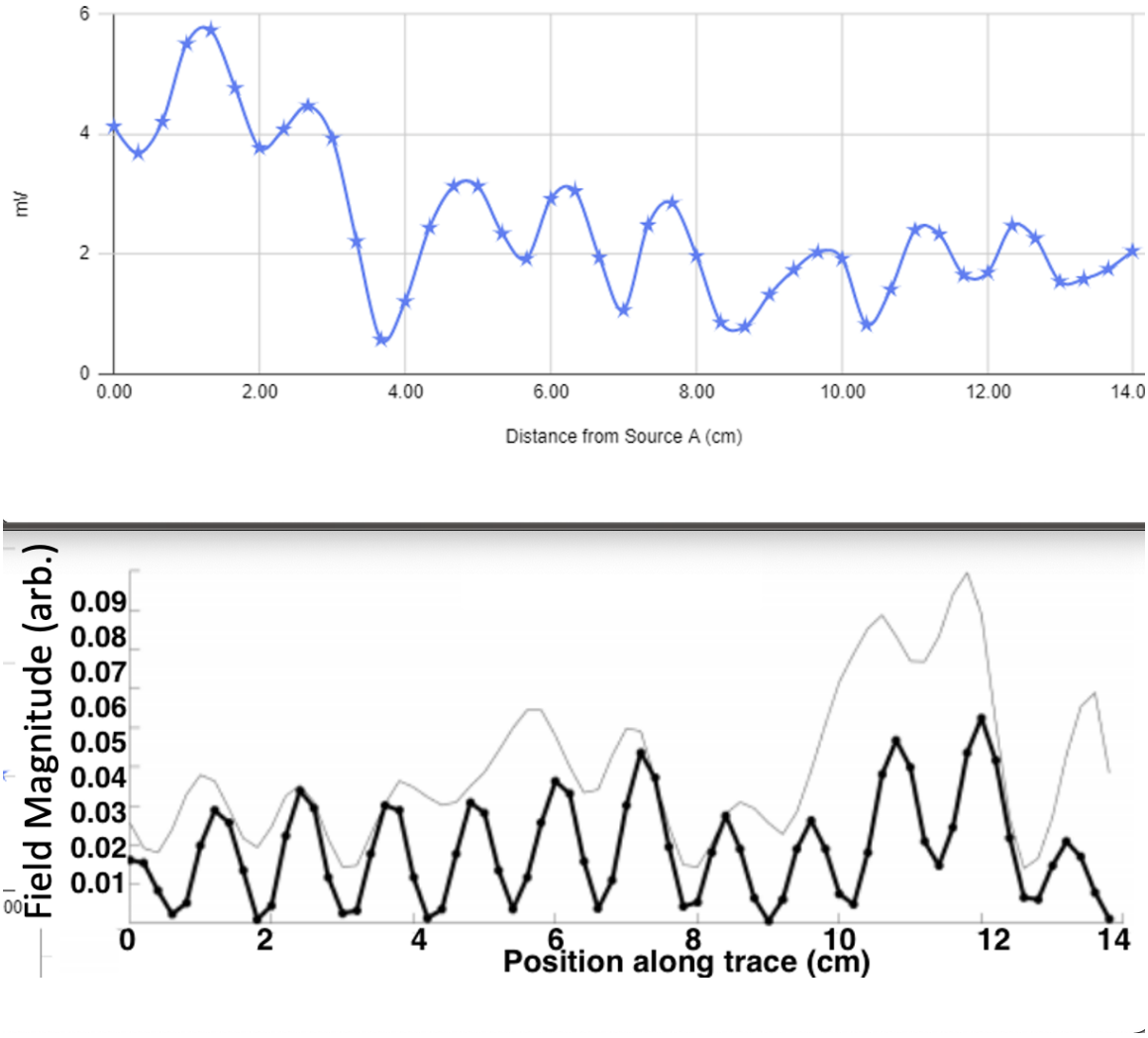


Figure 3.9: Microwave lattice measurements with power balancing. Above: Microwave lattice measurement that I took with power balancing of 5/10 dBm. Wavelength of the actual field is half the wavelength of the data taken in the spectrum analyzer. It has an approximate wavelength of 3.50 cm, which is longer than what was expected from the simulation shown in Fig.3.6. The plot shows the data points taken as well as a guide line to the eye (not a fitted curve). Below: Microwave lattice data taken by Andrew Rotunno and Doug Beringer in 2020 on a similar set-up as in this report. The approximate wavlength is 2.5 cm, which is closer to the simulation wavelength of 2.18 cm. This data set matched previously taken data a little more as a standing wave with a shorter wavelength. However, the old setup still has a shorter wavelength and the data collected still is a bit variable. It is important to note that on the data we took (left) the vertical error bars represent standard deviation which was very low between the trials we took, suggesting that the differences in the data from my setup and the old one is possibly due to differences in the pickup coil (e.g. orientation) and the power balancing.

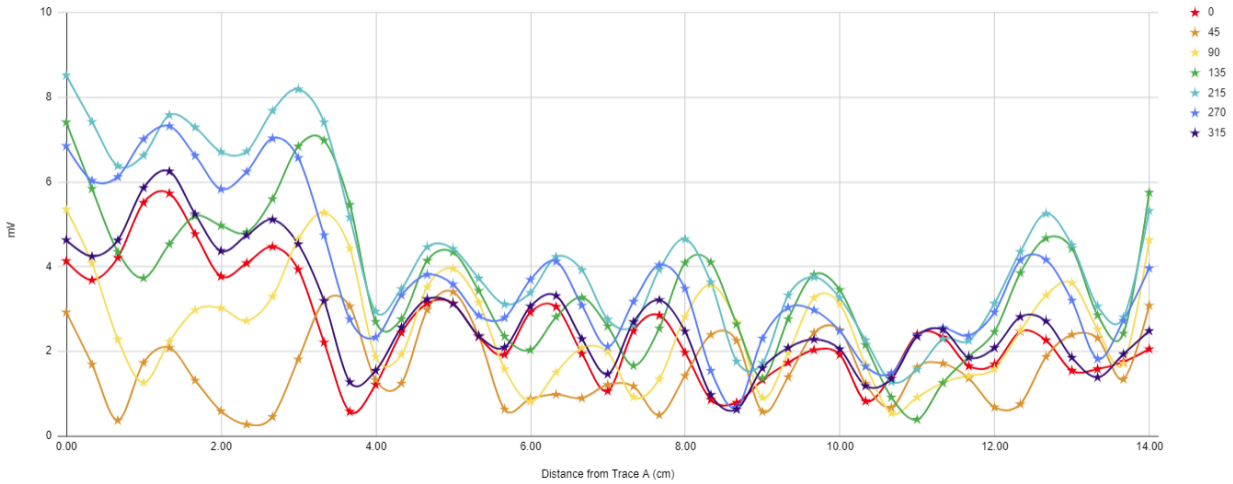


Figure 3.10: Microwave lattice amplitude for various relative phases (between sources A and B). This data set shows the magnetic field strength signal (as measured by the blue pickup coil) of the microwave lattice formed with sources at different phases of $0, 45, 90, 125, 215, 270, 315$ degrees shown here from red to purple. The plot shows the data points taken as well as a guide line to the eye (not a fitted curve).

The data in Fig.3.10 shows a cycle of the lattice shifting downward, back up and down towards the phase 0 lattice. Additionally, unlike previous trials, the waves maintain overall similar wavelengths despite changing the phase, which is a good indicator of power balancing and the improved reliability of the measurement scheme. Nevertheless, the standing wave structures in Fig.3.10 are not as regular as the sine wave expected from the standing wave theory in section 2.5.

## 3.3 Material Testing on the Trace

As shown in the previous subsections (see Fig.3.2.3.9,3.10), the standing wave has significant amplitude variations over the length of the microstrip trace. Based on past work by Andrew Rotunno and Doug Beringer and my own work, this spurious but significant structure is thought to be due to the probe itself, which can reflect the microwaves and disrupt the lattice. Before building a new kind of sensor, it is crucial

to run tests on the effect of various material on the output of the spectrum analyzer to see which materials have potentially minimal effect on the magnetic or electric field measurement results of the lattice. One issue with the method is the use of the blue cable pickup coil in order to run the material test: the data could be affected by how the material interacts with the blue cable pickup coil. We minimize the effects of the blue cable pickup coil by keeping it immobile, i.e. parked at a fixed location along the microstrip trace. Our approach is a good initial and qualitative assessment of the potential of various materials to make new pickup coils, dipole antennas, and fiber-based electric-optical sensor.

For the material trials, we used the same setup as Figure 3.1. We added a raised platform next to the board to use as reference to hover each material at the height of the platforms above the trace. Using the data from the 215° trial shown in Figure 3.11, We parked the pickup coil at $z = 3.7$ cm from trace point A, which was shown to be a point of maximum change on the graph. We also placed the materials around $z = 3$ cm from the trace as that was shown to be a location of maximum magnetic field amplitude. The reasoning for the setup is to place the material in an area on the trace that will cause the maximum change in the analyzer's measurement. Because the maximum changed for various phases we ended up moving the material $z = 3$ cm until finding the spot that changed the reading the most, in order to determine the largest possible effect of a material on the pickup coil reading.

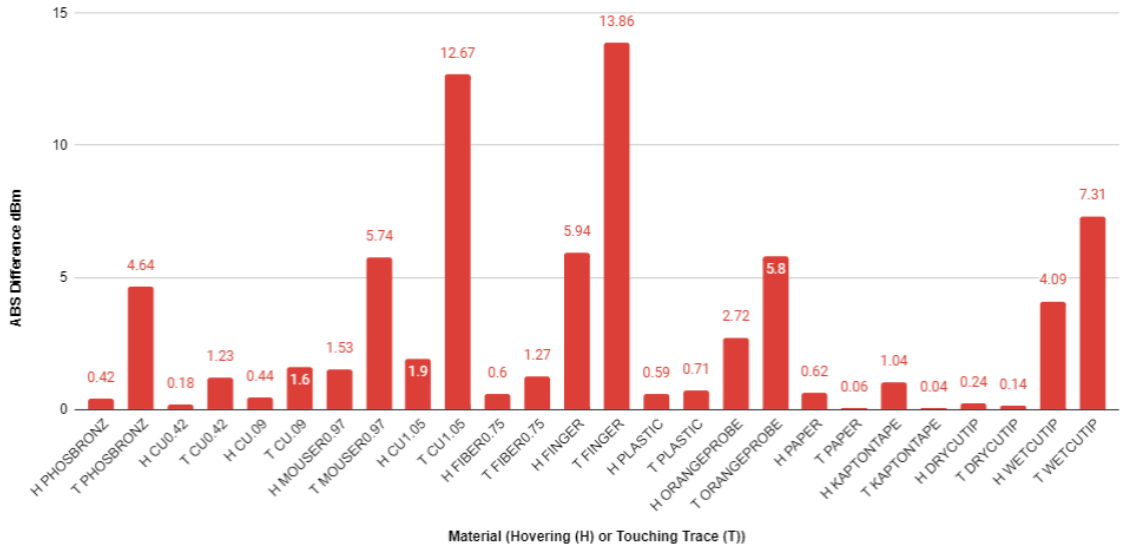


Figure 3.11: Effect of various materials on the microwave lattice. Each material was first hovered above the trace at the same height by placing it at the height of the platform and then touched the material to copper trace. In both instances, we moved it slightly varying from $z = 3$ cm from source point A to find the maximum possible difference between the output reading with no material and with this particular material graphed here as the absolute difference in dBm.

Though we did use a platform, there still is slight variability in the exact heights and orientations of the material due to my own error in properly holding the material straight and perpendicular to the direction of microwave travel. Despite this variability, the signal differences are a good indicator of which materials have minimal effect on the magnetic field output and, therefore, will be good candidates for materials for probes to be built from. There was an overall trend of increase in effect with increase in copper diameter (with some discrepancies). The purpose of the wet cutip gave a good indication that the large effect due to a finger could have to do with moisture. Optical fiber, with a low hovering effect of (0.6 dBm), shows promise for a fiber-based electro-optic sensor. Likewise, a sensor based on very thin copper wire should also minimize unwanted microwave reflections.

We then repeated the material testing for just wires, and we ensured a more accurate approach by having raised platforms on both sides of the trace at the same height, in order to properly place wires at the same hovering height above the traces. The results are shown in Fig.3.12.

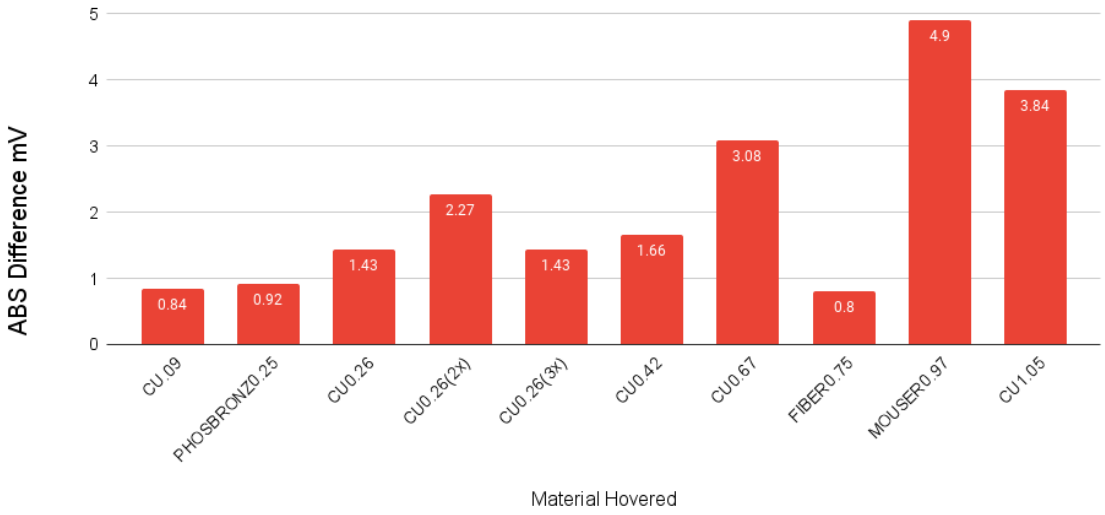


Figure 3.12: Wire effect on pickup coil reading. Each wire was hovered above the trace at the same height by placing it stretched perpendicular across the trace with ends at platforms of equal height of approximately 1 mm above trace. Furthermore, we moved the wire slightly around the $z = 3$ cm position (from source A) to find the maximum possible the maximum possible difference between the output reading with no material and with this particular material graphed here as the absolute difference in dBm. The labels represent different materials with diameters given in mm. "Mouser" is a specific brand of thin coaxial cable with an insulating cladding on top of the wire. Cu0.26(2x) and Cu0.26(3x) represent 2 and 3 Cu0.26 braided together respectively as shown in Fig.3.13.

Figure 3.13: Cu0.26 wires used in Fig,3.12. The top wire is just one copper wire with 0.26 mm diameter. The middle wire consists of 2 CU0.26 wires hand-braided, and the bottom wire consists of 3 Cu0.26 wires hand-braided.

From Fig.3.12, we can conclude that generally speaking there is an increase in the effect of the wire (or cable) as the thickness of the conductor is increased. There seems to be also an effect due to the spatial makeup of the wires, as Cu0.26(3x) had less of an effect compared to Cu0.26(2x) perhaps due to more gaps within an area of the wire from braiding.

## 3.4 Fabrication of a Magnetic Field Sensor Using "Mouser" 0.97 mm Cable

As concluded by the material test, smaller diameter cables and wires tend to produce less of an effect on the readings. We first fabricated a pickup coil from the thin "Mouser" coaxial cable with diameter 0.97mm, which had a larger effect than the

thinner copper wires, but had a lower diameter than the original blue pickup coil as shown in Fig.3.12. The "Mouser" wire refers to the 50 Ohm coaxial cable (manufacturer: Taoglas, part #CAB.721) with the following dimensions, per the datasheet: inner conductor (silver-plated copper) with diameter 0.22 mm, FEP dielectric with diameter 0.70 mm, ground braid shield (silver-plated copper) with no specified diameter, and the insulating FEP jacket with diameter 1.32 mm [11]. The pickup coil was fabricated from the cable, using a razor blade to expose the inner conductor at one end by removing the outer conductor braided sheath. Using tweezers, the wire was bend into a loop of 1.7mm diameter and soldered to the outer conductor (Fig.3.14).

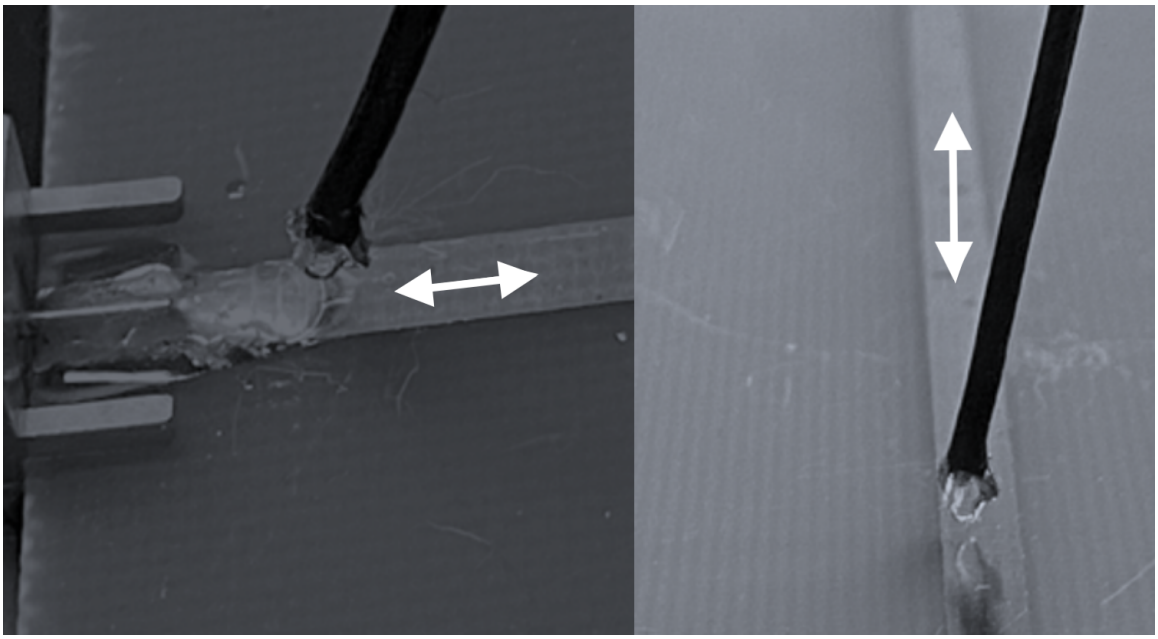

Figure 3.14: Pickup coil for magnetic field measurements based on the "Mouser" coaxial cable. By the RHR, the maximum magnetic flux occurs when $\hat{n}$ of the loop is perpendicular to current direction (arrow) (left), while the flux is minimized when $\hat{n}$ is parallel to the current axis(right). These orientations are as defined in Fig.3.3. The coil depicted has a diameter of 1.7 mm.

Using the same methods for power-balancing as shown for the blue-pickup coil, with the pickup coil first perpendicular to the trace's current, we found a proper

balance at 8.7 dBm for source A and 10 dBm for source B.

We proceeded to see if there was a translation in the standing wave when the phase between source A and source B was shifted $0, 90, 180, 270$ degrees (Fig.3.15). As expected, there was a shift as the phase difference between the sources was cycled through. The average wavelength of 2.33 cm which is closer to the expected wavelength from simulation (Fig.3.6) compared to the blue pickup coil in my data and the previous one taken by A. Rotunno and D. Beringer in Fig.3.9.

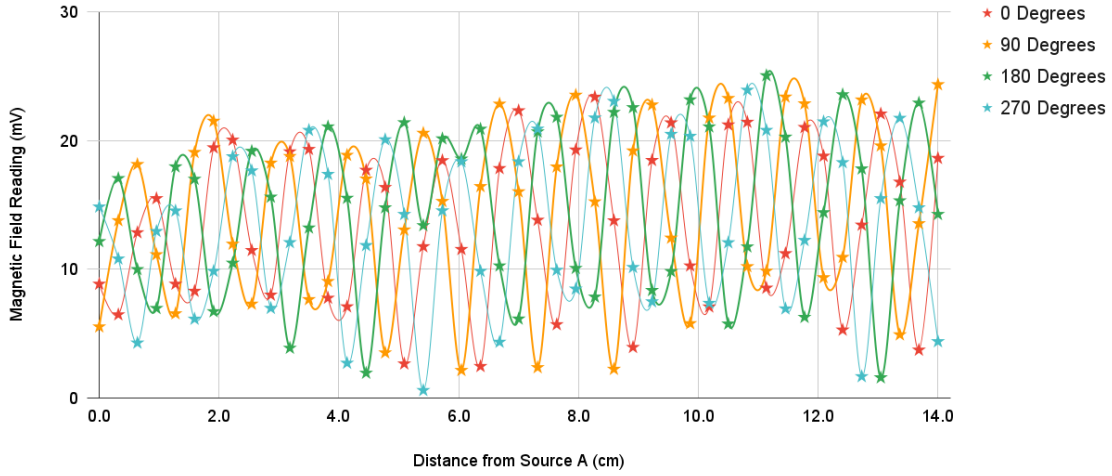


Figure 3.15: Magnetic field pickup coil signal from the "Mouser" pickup coil in mV along the trace. Compared to Fig.3.10, there is a clearer regular shift in the standing wave when sources are shifted from 0, 90, 180, 270 degrees out of phase with one another. Despite little shifts, the waves were relatively close to each other's amplitudes and ranges. Figure shows the data points taken as well as a guide line to the eye (not a fitted curve). The curves correspond to an approximate average wavelength of 2.33 cm, as the wavelength of the magnetic field would be twice of that of this plot. For the 180 degree curve (green) the standing wave has an unexplained "kink" in it in the region of $z = 5 - 6$ cm.

## 3.5 Fabrication of an Electric Field Sensor from "Mouser" 0.97 mm Cable

Using the same type of thin coaxial cable as for the "Mouser" pickup coil, we fabricated a small dipole antenna to detect the microwave electric field. We stripped off the outer protected sheath, and then moved all the braided outer conductor to one end, securing it together with solder. The inner conductor was bent in the opposite direction from the sheath, thereby producing the two poles. The length of the combined poles is 8 mm. We then measured the electric field by placing the poles orientation along the current as shown in Fig.3.16.

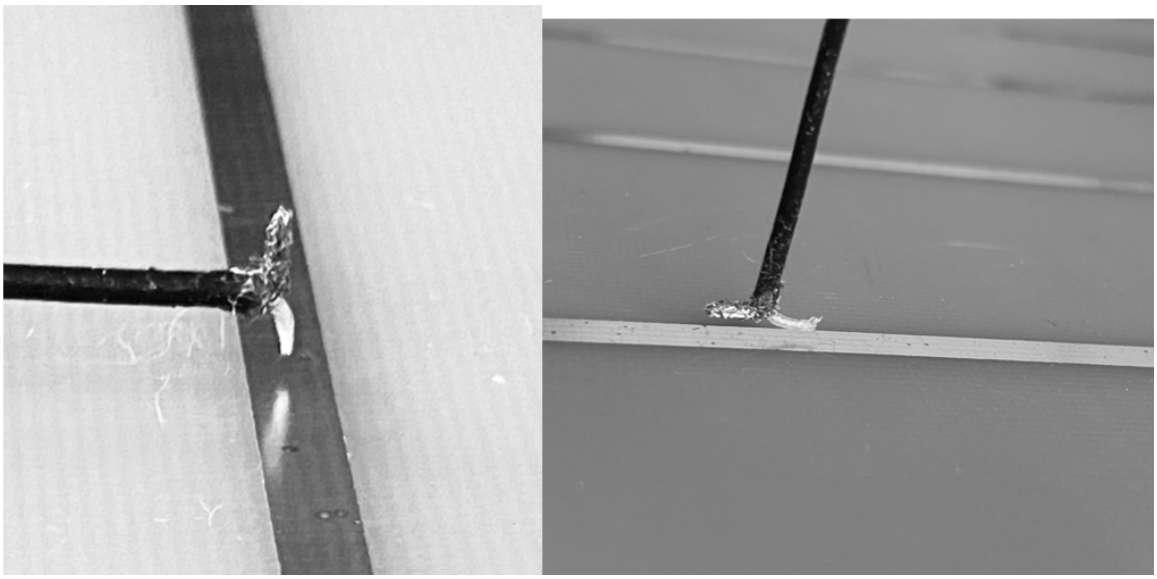

Figure 3.16: Mouser dipole antenna. The electric field was measured using the dipole antenna via the spectrum analyzer in mV. On the left is the setup where the poles' orientation are vertically perpendicular, to maximize the antenna's electric field response signal, while on the right the poles' orientation is along the current direction to minimize the electric field response. The length of the combined poles is 8 mm.

As shown in the theory section in Fig.2.5, the electric and magnetic field components should be 90 degrees out of phase with equal magnitudes for a microwave standing wave, but the electric and magnetic field magnitudes should be 180° out-of-phase. In Fig. 3.17, we expect to see the 180 degrees translation between the electric and magnetic field magnitudes as we are measuring power (see section 2.5). The EM lattice structures generated by the standing wave aligned somewhat with the theory. However, the dipole antenna had a larger amplitude range, highlighting the different sensitivities of the two sensors, while also suggesting that perhaps the poles need to be shorter, or the sensor was closer to the trace compared to the pickup coil.

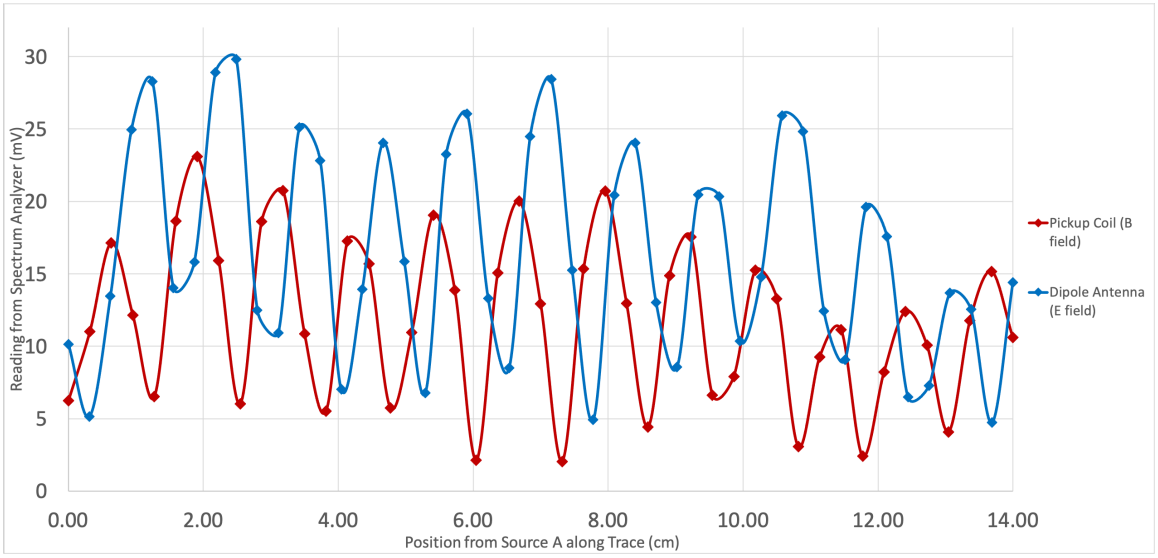


Figure 3.17: Magnetic and electric field strength measurements versus position for a microwave standing wave at 6.8 GHz using the Mouser cable-based pickup coil and dipole antenna. The electric and magnetic signals are roughly 180° out-of-phase, as the maximums of one aligned with the minimums of the other.The plot shows the recorded data points with lines as guides to the eye (not a fit). The electric field has roughly the same wavelength as the magnetic field of 2.33 cm, when we consider it to be twice the spatial period obtained from this plot.

## 3.6 Fabrication of a Magnetic Field Sensor Using a Copper Coaxial Cable with Inner Conductor Diameter 0.127 mm

As found in Fig.3.12, smaller diameter copper wires tended to have the least effect on the readings for the microwave system. Therefore, we used a 50 Ω semi-rigid micro-coaxial cable with a small inner conductor diameter of 0.127 mm and an outer conductor diameter of 0.584 mm (part #UT-020). In between the conductors, there is PTFE dielectric with diameter 0.432 mm [12]. As shown in Fig. 3.18, the pickup coil was fabricated in a similar manner to that for the "Mouser" coaxial pickup coil: by stripping the outer conductor and dielectric and fastening the inner conductor stub into a loop. The stub end was soldered to the outer conductor. The connection was verified by measuring a resistance over it. The magnetic field pickup signal was measured in mV along the trace with 45 data points points along the 14 cm length of the trace, as shown in Fig. 3.19. Compared to Fig. 3.10, there is still a clear translation shift of the standing wave when sources are shifted from 0, 90, 180, 270 degrees out of phase with one another. There is not much difference between this figure and that of the "Mouser" pickup coil (Fig.3.15). Despite little shifts, the waves were relatively close to each other's amplitudes and ranges.

We also verified that the pickup coil was essentially measuring the magnetic field: as shown in Fig. 3.20, when we rotated the coil area to point along the current direction, the pickup coil signal dropped significantly, i.e. down to 1 mV in the central section of the trace compared with a roughly 10 mV signal with the coil aligned perpendicular to the current axis. However, the pickup signal remained relatively high at the trace ends (3-4 mV), likely due to distortion of the microwave field by the connectors and spurious coupling of the pickup coil to the connectors.

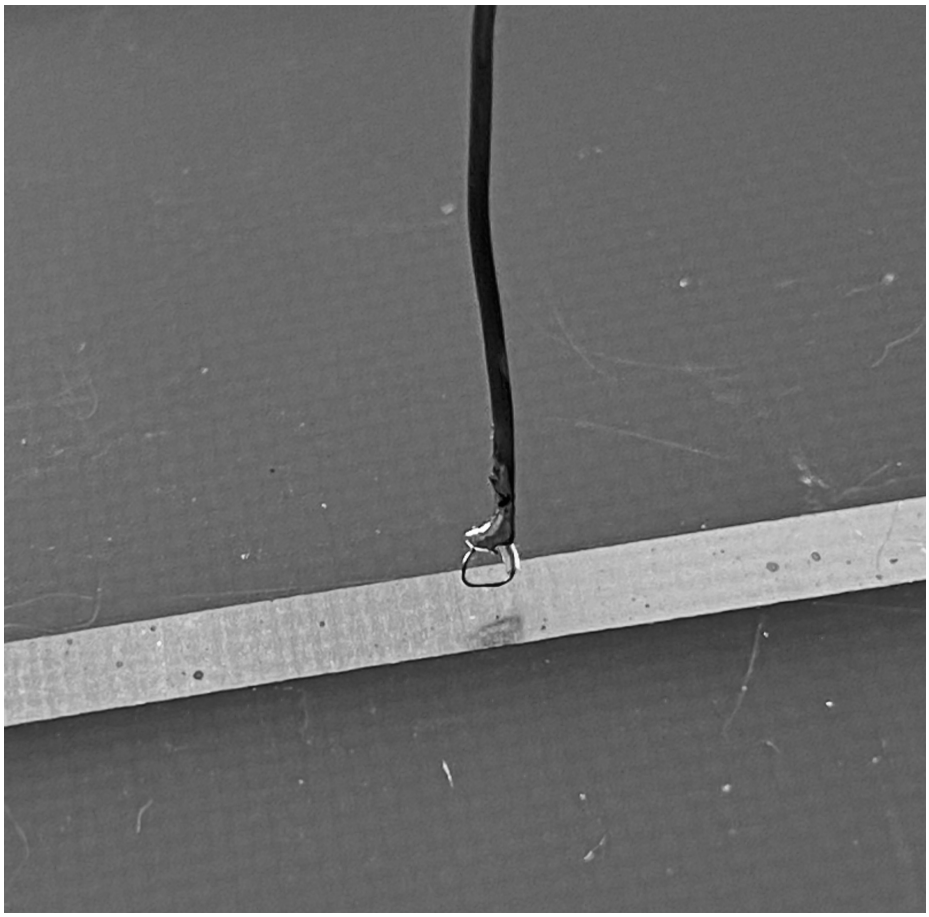

Figure 3.18: Pickup coil from the 0.127 mm copper micro-coax cable fastened perpendicular to the current direction for maximum magnetic field sensing. The pickup coil is roughly circular and has a diameter of about 1.4 mm.

## 3.7 Fabrication of an Electric Sensor Using a Copper Coaxial Cable with Inner Conductor Diameter 0.127 mm

Similar to the "Mouser" dipole antenna, we created a dipole antenna based on the micro-coaxial cable to measure microwave electric fields. The outer conductor was stripped on one side of the tip of the cable, and the other side was fastened together and extended outward. Then the dielectric was stripped off, and the inner conductor was bent outward opposite to the outer conductor. Figure 3.21 shows the micro-

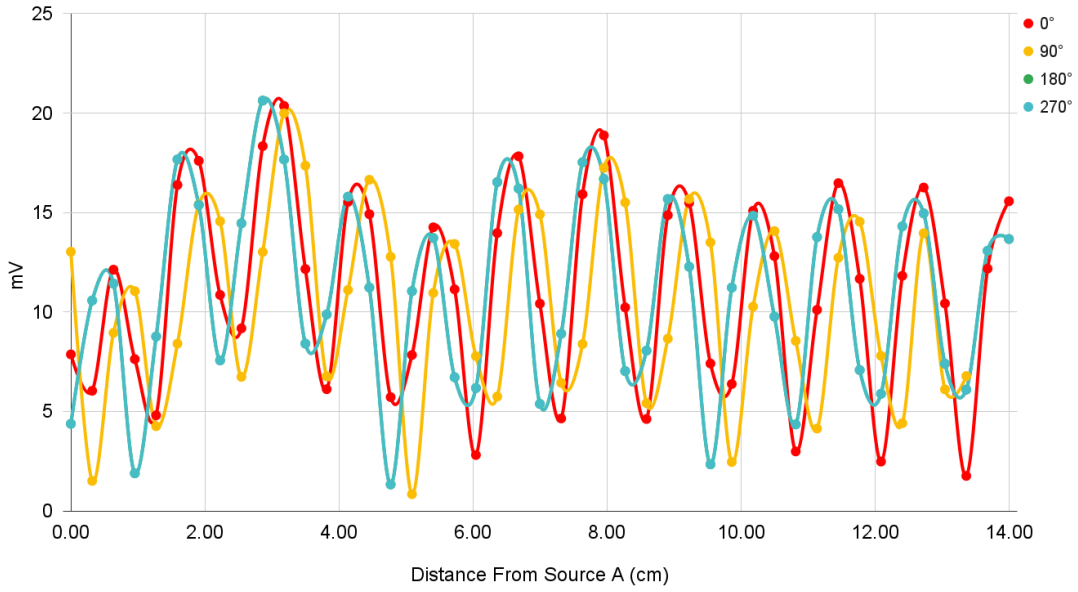


Figure 3.19: Microwave lattice pickup coil signal versus axial position along the trace for the magnetic pickup coil based on a micro-coaxial cable. It is important to note here that for the 180 degrees out of phase curve (green), the standing wave is held in the center unlike in Fig. 3.15. Twice the plot's wavelength corresponds to the measured field strength of the magnetic field's wavelength which is then roughly 2.54 cm, which is closer to simulations compared to my data for the blue coaxial cable pickup coil (Fig. 3.9) but farther off than from the "Mouser" micro coaxial cable (Fig. 3.15).

coaxial cable dipole antenna.

Again we wanted to show that the experiment aligns with the theory with magnetic and electric lattice structures 90° out of phase, which would show up as 180 degrees. The microwave lattice data obtained with the micro-coax dipole antenna (see Fig. 3.22) is a little less uniform than the equivalent data using the "Mouser" dipole antenna. Possible reasons for this are discussed in the conclusion.

Finally, we wanted to see if we were truly measuring the electric field by observing if the reading disappears when we switch the dipole antenna to the minimum field sensitivity orientation. The results are shown in Fig. 3.23. Though the electric field

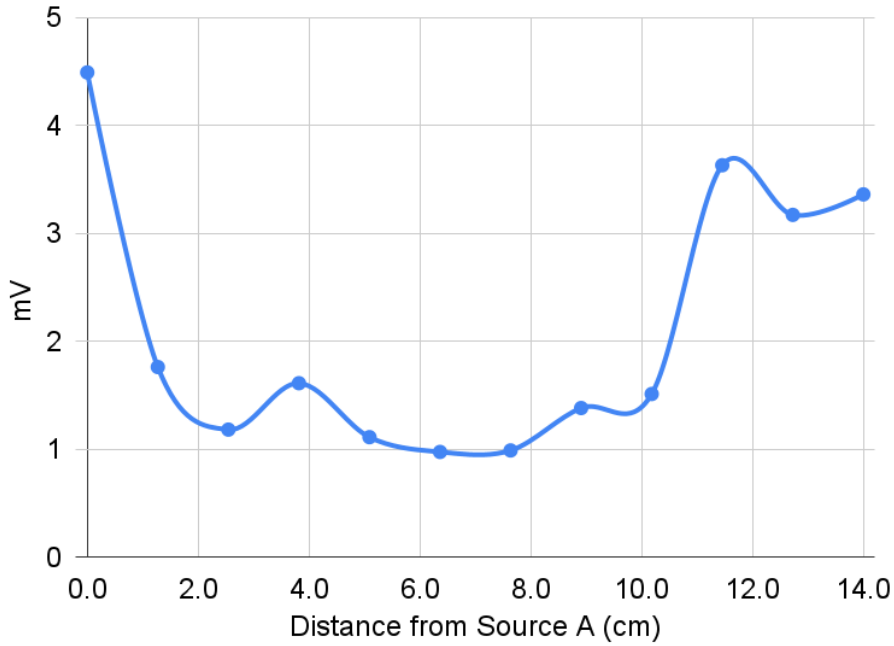


Figure 3.20: Data for pickup coil area along current trace axis (minimum sensitivity orientation). Here the sources were 0 degrees out of phase. The standing wave disappears and the magnitude drops by about a factor of 10 in the central portion of the trace.

strength signal did not disappear to 0, the magnitude does drop significantly in Fig 3.23.

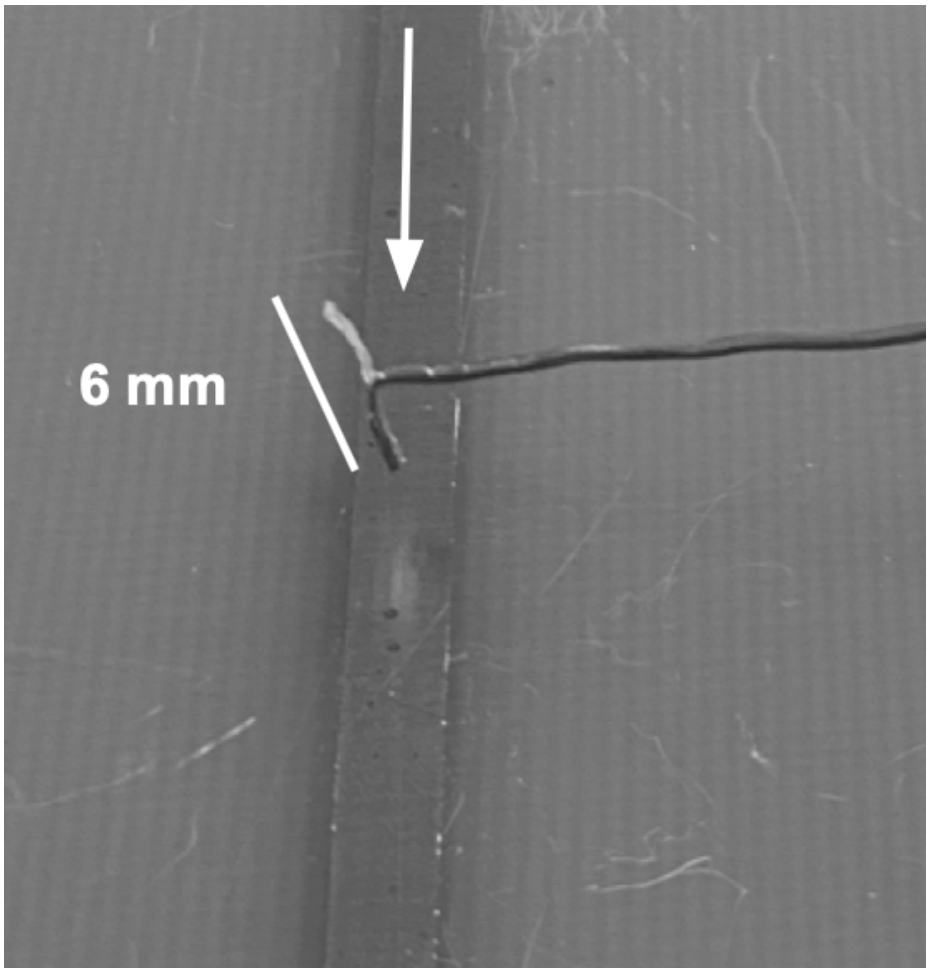


Figure 3.21: The electric field strength was probed using the dipole antenna oriented along the current direction via the spectrum analyzer in mV. The poles are vertically perpendicular to the current direction.

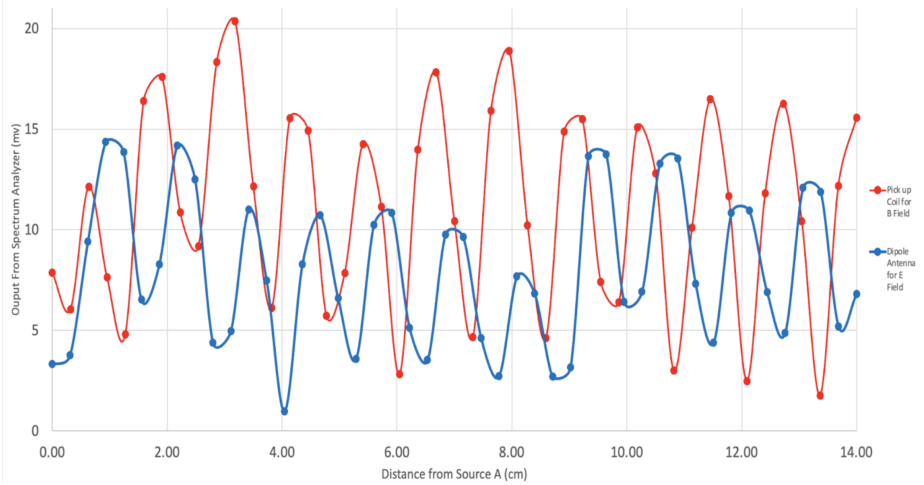


Figure 3.22: Measurements of the microwave lattice (versus position along the trace) with the micro-coaxial cable pickup coil and dipole antenna. The lattices became closer to 180 degrees out of phase as we move farther from source A. The wavelength of the electric field corresponds to twice the wavelength of the blue line. Therefore, the wavelength for the electric field was shorter than that for the magnetic field of 2.33 cm compared to 2.54 cm.

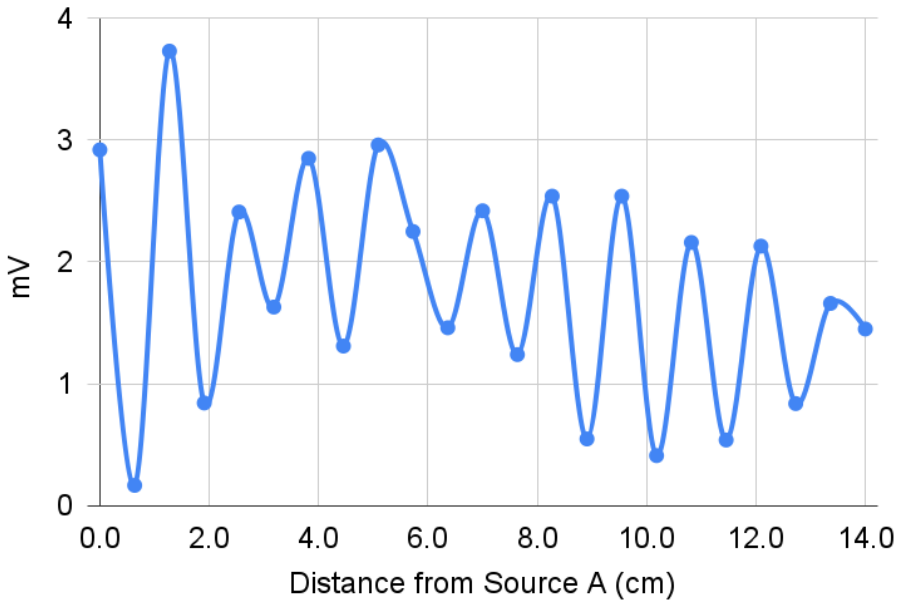


Figure 3.23: This data was for the dipole antenna with the poles along the trace (minimum electric field sensing orientation). The signal did not go to zero, suggesting it is not purely measuring electric field. However, the magnitude readings did significantly decrease compared to the maximum electric field orientation.

# Chapter 4

# Design and Simulation of a Micro-coaxial Cable-to-CPW Connection

This chapter describes computer simulation-based research on the transfer of microwaves from a coaxial cable to a co-planar waveguide (CPW) and vice versa, which is essential for injecting microwaves into the atom chip (and also for giving them an exit port). Furthermore, in the context of the micro-coaxial cable based sensors of the previous chapter, a method is needed for directing signals from a micro-pickup coil e.g. from the 80 micron-scale center conductor of a UT-013 micro-coax cable) into a larger diameter coaxial cable transmission line that can be connected to a spectrum analyzer (1-2 mm diameter cable). Conveniently, a tapered coplanar waveguide transmission line can focus or expand the size of a microwave spatial mode. Thus there are two main structures to design and simulate: 1) a coaxial cable to coplanar waveguide connection and 2) a tapered coplanar waveguide. A basic model for the coplanar waveguide is shown in Fig. 4.1

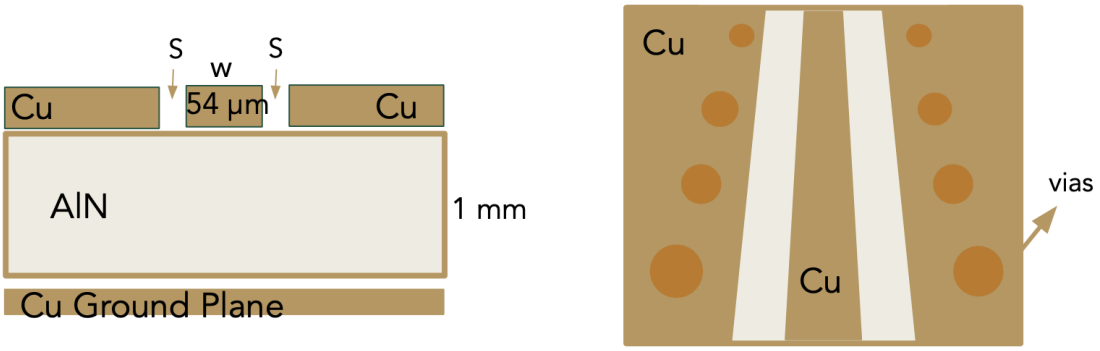


Figure 4.1: Basic layout of a coplanar waveguide (CPW). Left: Side view of CPW. We use a dielectric such as Aluminum Nitride (AlN) or FR4 with a copper trace width width ($w$) and a separation width ($s$) of exposed dielectric as a boundary to the side copper plates. On the bottom there is a copper groundplane. Right: Top view of a tapered CPW. The dark disks in the top view are vias, which are copper tubes connecting groundplanes to the bottom ground plane. The vias act as a fence that prevents leakage of the CPW microwave field away from the center trace and into the region of substrate sandwiched between the top and bottom groundplanes.

## 4.1 Coaxial Cable to Straight CPW

A coplanar waveguide (CPW) is a transmission line that consists of a center trace (width $w$) and two conducting ground planes on the top surface of a dielectric substrate. Two gaps (width $s$) on either side of center trace separate it from the top ground planes, which are connected with metallized vias (holes) to a third conducting ground plane that covers the entire bottom surface of the substrate.

Figure 4.2 shows a micro-coaxial cable-to-CPW connection that is modeled with the microwave simulation software FEKO (by Altair Inc.). In order to make the transfer of microwaves from the cable to the CPW as efficient as possible (i.e. minimize reflections), a 50 Ω impedance must be maintained throughout the transfer structure. The simulations encompassed here involves a CPW, which we designed previously, and which we used as a starting point to determine the optimal and sim-

plest way to transfer microwave signals efficiently to and from a micro-coaxial cable. All of the planar conductor elements on the CPW consist of 5 micron thick copper. The 10 mm long micro-coaxial cable's configuration dimensions were setup using an online theory-based calculator ([13]) and is made from an inner conductor (radius 0.027 mm), covered by a polyethylene insulator (dielectric constant $\epsilon = 2.25$ and radius: 0.0945 mm), with a conducting sheath on the outside. The CPW uses an aluminum nitride substrate (thickness = 1 mm, dielectric constant $\epsilon = 8.9$) with a copper ground plane, and copper center trace separated on both sides from the top ground planes. The center trace is directly connected to the inner conductor of the micro-coaxial cable. Two rectangular cuboid copper connectors on either side of the coaxial cable connect the outer conducting shell of the cable to the copper planes on either side of the trace, as illustrated in Fig. 4.2. We ran simulations of the device at frequencies from 1-15 GHz and saw good current flow and power transfer for each. The outer end of the cable is a 50 $\Omega$ source and the outer end of the CPW is a 50 $\Omega$ load resistor.

We proceeded to check for a proper impedance of around 50 $\Omega$ and low reflection coefficient. While the impedance is roughly 50 $\Omega$ at low frequency, it diverges from this value at higher frequencies. The periodic structure in the impedance plot (and reflection coefficient plot) suggest that there is an impedance matching issue in the model, either at the cable-CPW interface or at the CPW edgeport (load port) or the cable edgeport (source port) (Fig. 4.3). Simulations by other lab researchers have identified additional structures that must be added to the CPW source and load ports for proper coupling into the CPW.

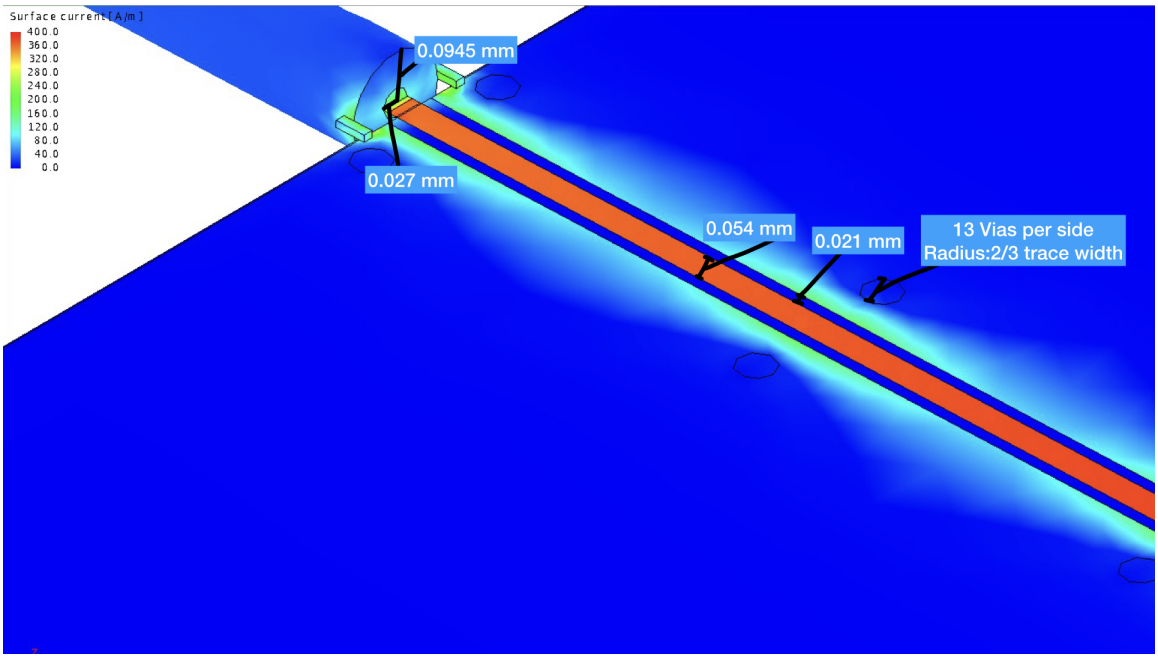


Figure 4.2: Coaxial cable-to-CPW connection model. This connector has good power and current transfer efficiency. We used a CPW model with a 10 mm × 10 mm aluminum nitride substrate with 13 vias (circles) which help guide the current through the trace (width: 0.054 mm).

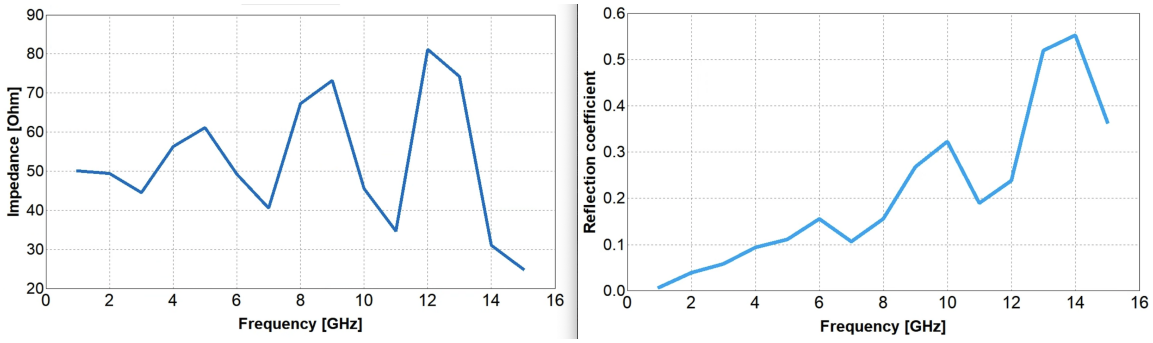


Figure 4.3: Impedance and reflection plots at 1-15 GHz for the coaxial cable to coplanar waveguide connection shown in Fig. 4.2. The reflection coefficient and the impedance calculations are generated by the FEKO simulation.

## 4.2 Tapered Coplanar Waveguides

Next, I studied a tapered CPW, so that microwaves can be inserted from mm-scale coaxial cables into the 50 $\mu$m-scale microstrip structures of an atom chip. This model also is useful for a potential smaller pickup coil and dipole-antenna sensor based on much finer micro-coaxial cable that require a tapered CPW to couple a very narrow microwave mode into the much larger microwave mode (mm-scale) of a regular coaxial cable connection into the SMA port of a spectrum analyzer. In making the tapered waveguides, I used an impedance calculator to find the proper separation widths ($w$ and $s$) needed for 50 $\Omega$ impedance. I designed the focused CPW using several decreasing linear trace width segments and corresponding seperation widths. I found that at a certain limit, you do not need to keep increasing the number of segments between the first and final trace width sizes.

Figure 4.4 shows a model of the tapered CPW along with the current distribution in it. Figure 4.5 shows the impedance (centered on 50 $\Omega$) and the reflection coefficient for the tapered CPW structure for frequencies in the range of 1-15 GHz. The periodic behavior of the impedance and reflection coefficient point to a impedance matching issue (probably at the input and output edgeports).

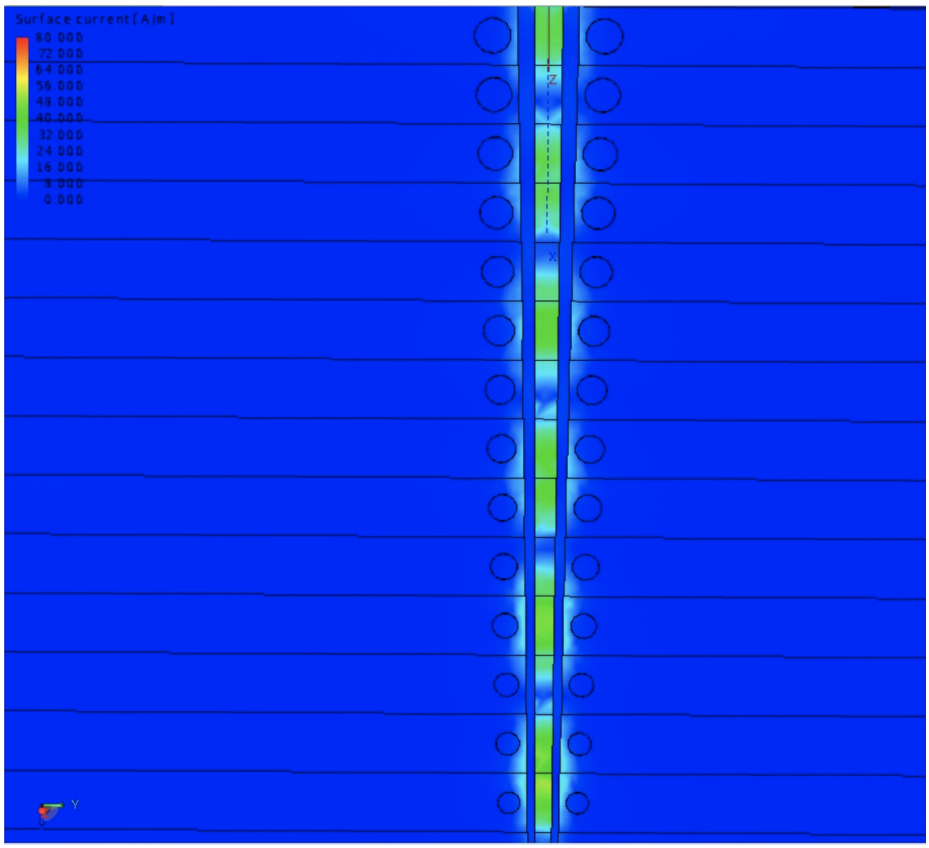


Figure 4.4: Microwave simulation of the current distribution in a tapered CPW from 0.75 mm center trace width to a 0.1 mm center trace width in 30 segments. The vias were made to have a radius that is 2/3 of the trace width at a given segment.

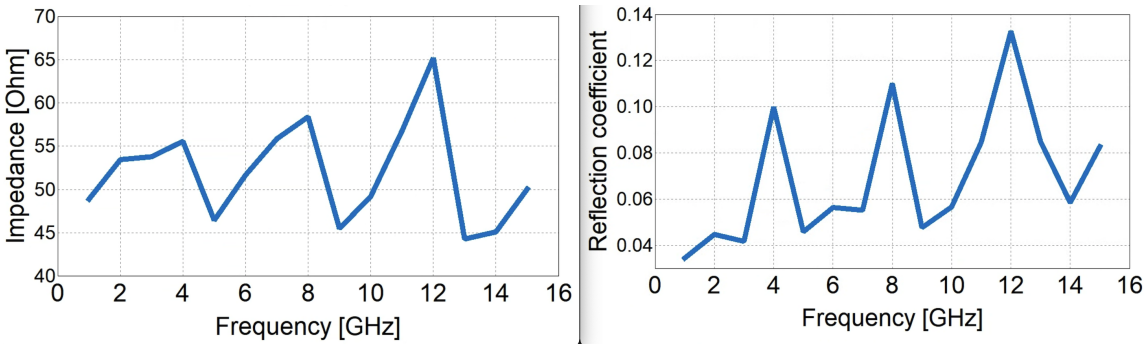


Figure 4.5: Impedance and reflection coefficient for the tapered CPW model in Fig. 4.4. The reflection coefficients were overall low ranging from 0.04-0.13 while the impedance varied between 45-65 Ω. These are both very similiar to the ranges for the non-tapered waveguide in 4.2

## 4.3 Microwave Simulations Conclusion

Both the microcoax-to-CPW connection and the tapered CPW model show promising results with significant power transfer and limited reflections for frequencies 1-15 GHz. However, additional simulations are needed to investigate the transmission of microwaves from a micro-coaxial cable (Microstock-inc.com, part # UT-013 with inner conductor: 0.08 mm) to a tapered CPW and then back to a larger coaxial cable. This coaxial cable is intended for connection to a spectrum analyzer. This architecture is necessary for optimizing the signal transfer from the sensor to the spectrum analyzer.

Additionally, the work presented here and work by others in the lab indicate that coupling microwaves into the atom chip via a coaxial cable-to-CPW-to-microstrip interface is capable of providing impedance matching and a low reflection coefficient – however, more simulations are needed to finalize these results and generate a final design.

# Chapter 5

# Conclusions and Outlook

This chapter summarizes the main conclusions of the thesis research on 1) measurements of the electric and magnetic field strengths of a microwave standing wave and 2) the simulation and design of a coaxial cable-to-CPW connection and a tapered CPW. This chapter concludes by providing an outlook for future work based on advances presented in this thesis.

## 5.1 Magnetic and Electric Near Field Probes

### 5.1.1 Powerbalancing

Power-balancing the microwave sources is crucial in order to observe the standing wave (microwave lattice) needed for proper trapping potentials used for the microwave atom trap. Though the phase checking method and the power balancing method at the trace center were positive in their improvements to the measurement of a standing wave, the results were still not optimal. There is still some failure of reproducibility, as parking the sensor at slightly different locations near the center has very variable power balancing results. As the pickup coils got smaller, the change in power between the two sources became less in order to produce a standing wave, indicating that the readings are affected by interference with the probe, though to a lesser extent with smaller probe cables.

### 5.1.2 Pickup Coils

Another indicator of problematic behavior is if the orientation of the pickup coil has no effect on the magnetic field reading. The original blue pickup coil, had no change in reading when we changed the loop's orientation from maximum to minimum magnetic field orientation. This further indicates problems with the pickup coil, perhaps measuring a combination of electric and magnetic fields, as well as interference between the coil and the trace. The use of a standard sized coaxial cable is non-ideal to measure magnetic and electric fields of a copper trace, as it is a large conductor and therefore, it could be actually measuring an interference interaction between the microwaves, trace and coil. The measured wavelength for the blue coaxial cable probe after power-balancing was roughly 3.50 cm, which is significantly longer than the 2.18 cm wavelength observed in simulation.

The results of the material test indicated that the smaller the diameter of material, the less effect it has on the microwave lattice system. Therefore, we fabricated new pickup coils from the "Mouser" wire (diameter 0.97 mm) and the copper micro-coaxial cable (diameter 0.127 mm) and found that the resultant magnetic fields measurements mimicked a standing wave. Additionally, we found that when we turned the copper micro-coaxial coil so that its area's $\hat{n}$ points along the trace, we saw a significant decrease in the magnitude of the reading, in the center portion of the trace, from average of 10 mV down to about 1 mV aligning with the right hand rule, and our assumption that we are measuring magnetic field. The "Mouser" pickup coil's readings had a wavelength roughly closer to simulation of 2.33 cm while the micro-coaxial probe's readings had a wavelength of 2.54 cm. However, the readings for the micro-coaxial probe followed a smoother standing wave pattern. Variations in the results could be

due to unconsidered factors such as how far the probe was from the trace as well as the size of the loop's effect on the reading for a particular wire.

### 5.1.3 Dipole Antenna

Based again on the material test results, we also fabricated dipole antennas from the "Mouser" wire and the copper micro-coaxial cable. Both probes measured the electric field strength of the microwave standing wave. Additionally, both probes measured a wavelength of roughly 2.33 cm which is closer to the simulation wavelength of 2.18 cm. For the copper micro-coaxial cable dipole antenna, changing the dipole orientation to that for minimum electric field sensitivity did not make the electric field signal go to 0, but did significantly decrease the magnitude of the reading. There are some factors that could have led to this behavior including the poles not being exactly the same size, as well as the overall length of the poles, and and the sensor distance above the trace. Another possibility could be that the microstrip's microwave mode is quasi-TEM, and therefore, the electric field could have a very small component parallel to the trace. This could explain the small axial standing wave component picked up by our dipole antenna. Additionally, we showed that the magnetic and electric field magnitudes were about 180° out-of-phase spatially, which is expected for electric and magnetic fields that are 90° out-of-phase. Furthermore, we observed the translation of the standing wave along the trace as the phase difference between the two sources was increased.

There are several more tests to be taken to optimize the sensors. First, for the mouser and the copper wire trials, the amplitude changed between the pickup coil and the dipole antenna, suggesting that in each case, the sensors were not placed at the same level from the trace. Additionally, it could mean that the dipole antenna

was not the proper length, or that it may not have had equal length poles. Finally, to optimize the system it would be interesting to try an even smaller wire for our sensor. The next wire would have a inner conductor diameter of 0.08 mm (microstock-inc.com part # UT-013). This wire does not have an attached SMA connector, and will need a tapered coplanar waveguide to connect it to the spectrum analyzer, as mentioned in section 5.3.

Overall, we have shown that microwave traveling waves of equal power and opposite propagation direction along a trace produce a microwave standing wave in which the electric and magnetic power components are roughly 180 degrees out of phase, as expected for electric and magnetic field components that are 90 degrees out of phase. Therefore, once the fabrication of the microwave atom chip begins, the pickup coil sensor will be useful for measuring the strength and location of the magnetic minimas in order to characterize where the atoms will be trapped axially.

## 5.2 Microwave CPW Simulations

We were able to obtain reasonable current and power transfer with promising low reflections and roughly close to 50  impedances for the microcoax-to-CPW connection and the tapered CPW model. However, more tests are needed to investigate why there are significant "resonant peaks" in the impedance. These unwanted peaks could possibly be suppressed by an improved termination of the CPW at its edgeports or by using coax-to-CPW connections at the source and load. The next step in the tapered CPW model is to include connections to a mm-scale coax cable on one end and to a micro-coax cable on the other end. The continued development of the tapered CPW will be necessary to have optimal signal flow between the possible sensor from the micro-coaxial cable (Microstock-inc.com UT-013 with inner conductor: 0.08 mm) to

the spectrum analyzer. Additionally other researchers in the lab have found additional methods for proper current and power transfer that should be implemented into the next simulation including having a row of vias at the source and load edgeports as well as groundwalls on either side for optimal current transfer.

## 5.3 Outlook for the Future

Microwave lattices can be used for axial confinement of atoms within the microwave AC Zeeman trap formed from three parallel microstrip transmission lines. The work presented in this thesis shows that applying equally-powered current to both ends of a trace produces multiple axial low field regions (for low field seekers) that could potentially trap atoms. These minimums were shown to translate when the phase between the traces was changed.

Another possible application of microwave lattices is to manipulate macroscopic objects like microrings and microsphere. Stephen Rosene's thesis project focuses on microwave tweezers and this application. The simulations done for this thesis for coax-to-CPW and tapered CPW could be useful for coupling microwaves in the microstrips of the microwave tweezers. Additionally, the pickup coil could be used to map out the magnetic field.

A microwave pickup coil based on the copper micro-coax cable could be used for more experiments to measure the magnetic near field. For example, it could be used to measure the AC skin effect [9] if we operate the device at a lower frequency or use a thinner metallization on the microstrip. Additionally, one could confirm the microwave proximity effect in parallel microstrips by observing that parallel AC currents repel and anti-parallel AC currents attract. Finally, using two pickup coil probes, one could observe the hopping back and forth of currents between two parallel microstrips.

Finally, magnetic field sensors have biomedical applications in point of care devices as well as magnetocardiography, magnetotomography, magnetomyography, and magnetoneurography. There is an increasing need to make these devices more affordable while also reducing noise and improving spatial resolution by making the sensors smaller [14]. The microwave pickup coil developed here could be potentially used in these applications as well as a potential smaller coil from the smaller micro-coaxial cable (microstock-inc.com part # UT-013).

# Bibliography


[1] LIGO-a Gravitational Wave Interferometer. LIGO Laboratory. https://www.ligo.caltech.edu/page/what-is-interferometer

[2] R. Anderson, H. R. Bilger, and G. E. Stedman, "Sagnac" effect: A century of Earth-rotated interferometers, Am. J. Phys. 62, 975 (1994).

[3] W. Miyahira, A. P. Rotunno, S. Du, and S. Aubin, "Microwave atom chip design", DAMOP 2021 conference (online).

[4] W. Miyahira, A. P. Rotunno, S. Du, and S. Aubin, "Microwave atom chip design", MDPI Atoms 9, 54 (2021).

[5] S. M. Dickerson, J. M. Hogan, A. Sugarbaker, D. M. S. Johnson, and M. A. Kasevich, "Multiaxis inertial sensing with long-tim point source atom interferometry", Phys. Rev. Lett. 111, 083001 (2013).

[6] C.T Fancher, A.J. Pyle, A. P. Rotunno, and S. Aubin, "Microwave ac Zeeman force for ultracold atoms", Phys. Rev. A 97, 043430 (2018).

[7] C. Fancher, PhD thesis, "AC Zeeman Effect with Ultra-Cold Atoms", Dept. of Physics, College of William and Mary (2016).

[8] D. Jervis, MSc thesis, "Fabrication of an atom chip", Dept. of Physics, University of Toronto (2007).

[9] A. E. Blackwell, A. P. Rotunno, and S. Aubin, "Demonstration of the lateral AC skin effect using a pickup coil", Am. J. Phys 88, 676 (2020).

[10] P Sanghera, Chapter 6 - RFID+ Selecting the RFID System Design, RFID+ Study Guide and Practice Exams, https://doi.org/10.1016/B978-159749134-1.50010-4.(2007)

[11] Specification - mouser.com, (n.d.). https://www.mouser.com/datasheet/2/398/CAB.721-4307.pdf (accessed December 22, 2021).

[12] Show Data Sheet. (n.d.). https://www.microstock-inc.com/pdfshow01.php?item=UT-020 (accessed December 22, 2021).

[13] W.J. Highton, Coplanar waveguide with ground characteristic impedance calculator, Coplanar Waveguide With Ground Calculator. (n.d.). https://chemandy.com/calculators/coplanar-waveguide-with-ground-calculator.htm (accessed December 22, 2021).

[14] Murzin D, Mapps DJ, Levada K, Belyaev V, Omelyanchik A, Panina L, Rodionova V. Ultrasensitive Magnetic Field Sensors for Biomedical Applications. Sensors (Basel). 2020 Mar 11;20(6):1569. doi: 10.3390/s20061569. PMID: 32168981; PMCID: PMC7146409.